Comparison of different cross-sectional approaches for the structural design and optimization of composite wind turbine blades based on beam models

Edgar Werthen[1], Daniel Hardt[1], Claudio Balzani[2], and Christian Hühne[1]

[1]DLR German Aerospace Center, Institute of Lightweight Systems, Lilienthalplatz 7, 38108 Braunschweig, Germany
[2]Leibniz University Hannover, Institute for Wind Energy Systems, Appelstrasse 9A, 30167 Hannover, Germany

Correspondence: Edgar Werthen (edgar.werthen@dlr.de)

Abstract. During the preliminary ~~multidisciplinary~~ design phase of wind turbine blades, the evaluation of many design candidates in a short period of time plays an important role. Computationally efficient methods for the structural analysis are ~~needed to cover the required effects, e.g., correct prediction of~~ thus needed that correctly predict stiffness matrix entries for beam models including the (bend-twist) coupling terms. The present paper provides an extended overview of available approaches and shows their ~~ability~~ abilities to fulfill the requirements for the composite design of rotor blades with respect to accuracy and computational efficiency. Three cross-sectional theories are selected and implemented to compare the prediction quality of the cross-sectional coupling stiffness terms and the stress distribution based on different multi-cell test cross-sections. The cross-sectional results are compared with the 2D finite element code BECAS and are discussed in the context of accuracy and computational efficiency. The ~~most promising approach~~ analytical solution performing best shows very small deviations in the stiffness matrix entries compared to BECAS (below 1 % in the majority of test cases). It achieved a better resolution of the stress distribution ~~compared to BECAS and~~ and a computation time that is more than an order of magnitude ~~less computation time when the same discretization is used~~smaller using the same spatial discretization. The deviations of the stress distributions are below ~~10 percent for the~~ 10 % for most test cases. The ~~results can serve as a basis for the~~ analytical solution can thus be rated as a feasible approach for a beam-based ~~design~~ pre-design of wind turbine rotor blades.

1 Introduction

Beam-based approaches are commonly used in the conceptual and preliminary structural design of wind turbine blades. They are often embedded in a multi-disciplinary optimization (MDO) process (Scott et al., 2019; Serafeim et al., 2022) due to ~~their better~~ a superior computational performance compared to high-fidelity finite element (FE) ~~shell- or solid models~~models using shell and/or solid elements. A typical application ~~for an MDO is a~~ of MDO is the design of rotor blades with tailored bend-twist ~~reducing the aerodynamic loads as investigated by Scott et al. (2020) and Bottasso et al. (2012)~~coupling (Scott et al., 2020; Bottasso et al., 2
. The blade flexibility affects the angle of attack along the blade and thereby changes the lift and drag force distribution, reducing the flapwise bending moments. For the structural optimization in general, a common objective function is the reduction of mass or costs ~~Lee and Shin (2022)~~(Lee and Shin, 2022).

For larger blades, ~~according to the theory, the~~ mass and costs increase ~~proportionally to the cube of~~ to the power of around 2.4 with the blade radius (Rosemeier and Krimmer, 2022), whereas the annual energy production (AEP) increases proportional to the square of the blade radius ~~?. Faster growing~~ (Gasch and Twele, 2012). Hence, the blade mass and costs ~~compared to the AEPrequires the investigation of new technologies~~scale over-proportionally compared with the AEP. It is thus required to investigate new technologies, materials, or designs to withstand the increased mass-related loads and to limit the blade costs~~as~~ , which are a significant part of the overall turbine costs.

1.1 Beam models within the design process of wind turbine blades

The usage of beam models becomes necessary within the structural optimization in the preliminary design phase due to the evaluation of many design candidates~~in the preliminary design phase~~. The number of design candidates results from the investigation of different designs for the structural topology (e. g., number and/or positions of spars) and concepts for materials used and how they are combined in laminate lay-ups, which in turn have to be linked to a manufacturing concept. Consequently, ~~the~~ a basic requirement is a significant reduction of the computation time for model creation and the calculation of ~~internal~~ stresses compared to a high-fidelity FE model. The computation time for the stress calculation scales with the number of iterations of the optimization process. For the shell or solid FE model case, variations of the internal structure of the blade, e. g., the spar position, often requires a 3D CAD (Computer ~~added design~~Aided Design) model update and the subsequent translation into a new FE mesh. The higher ~~modelling~~ modeling effort and the longer computation times with 3D models are not acceptable in the preliminary design phase.

FE beam models require the input of accurate cross-sectional properties~~as input.~~, i. e., stiffness and mass matrices. In many design processes ~~(e.g., Scott et al., 2019; Wanke et al., 2021), these~~ (e. g., Scott et al., 2019; Wanke et al., 2021), the cross-sectional properties are determined ~~with the help of cross-sectional FE models to derive~~ using 2D FE models that serve to calculate the mass and stiffness properties and the stress distribution within the cross-section. These 2D FE approaches ~~have the same problems of an expensive model update~~ suffer from the need of expensive model updating, with re-meshing ~~when~~ in case the internal structure or layup changes ~~combined with a more expensive solving~~ during the optimization process, and from higher computation costs for solving the governing equations compared to analytical approaches.

1.2 Requirements ~~on~~ for an analytical cross-sectional approach

~~Based on the technologies described above (e.g., bend-twist coupling) that need to be investigated for the design of rotor blades, requirements for~~ Requirements for an analytical cross-sectional calculation module ~~can be derived~~ are derived in the following which serve to evaluate different calculation methods at a later stage. Composite blades are ~~modelled~~ modeled as beams with closed, different single- or multi-cell ~~cross-section geometries that can~~ cross-sections that vary along the beam axis. The parts of the blade~~e.~~, e. g., shell panels and spars, consist of different materials. Moreover, different materials within one part can occur. The structure of the blade is mostly thin-walled, except near the blade root~~and undergo~~ , and undergoes in-plane and out-of-plane cross-sectional deformations. Beside the classical loading of ~~thin beams like bending and~~ thin-walled beams such as bending or extension, shear forces play an important role ~~since they can be dimensioning for the design of rotor blades~~and

can be design-drivers. The couplings of the ~~beams~~ beam's degrees of freedom ~~due to the inner geometry~~ that result from the structural topology or the material layup have to be considered for an accurate representation of the blade. The computational efficiency, i. e., fast output with high accuracy, is of high importance as well to allow the assessment of ~~many~~ a large number of design candidates in the preliminary design phase.

The historical development of cross-sectional approaches for general beam structures is described by Hodges (2006). Chen et al. (2010) compare several existing tools for cross-sectional calculations~~(e.~~, e. g., "PreComp" ~~Bir (2006)~~ (Bir, 2006) or "VABS" ~~Yu (2007))~~(Yu, 2007).

1.3 Target setting

The present paper provides a comprehensive review of available cross-sectional approaches (section 2.4) based on the aforementioned requirements for the design of composite wind turbine rotor blades~~formulated above~~. Three cross-sectional theories are ~~then~~ selected (section 2.5) and implemented~~to compare the~~ . The results of the different methods, i. e., the cross-sectional coupling stiffness terms (e.g., extension-torsion, bending-torsion, section 3.2) and the stress ~~distribution in the cross-section~~ distributions in different cross-sections (section 3.3) ~~. A simple~~ are compared. A rectangular and a multi-cell airfoil-based cross-section serve as test cases. The focus is on the shear stress distribution caused by ~~transversal forcessince they~~ transverse shear forces, as these are more complex to calculate ~~and, among others, dimensioning for rotor blades as already described above~~compared to, e. g., bending-related normal stresses. The cross-sectional results are verified ~~with the 2D-finite element~~ using the 2D FE code BECAS (Blasques, 2012)~~and used also by the industry~~ , which is a well-established industry standard in rotor blade design and serves as a reference solution in this paper. A verification of BECAS itself ~~with VABS(also a 2D-FE beam cross-section code , (Yu, 2007))~~ using VABS, which is also a 2D FE code for the calculation of beam cross-sectional properties (Yu, 2007), is given in Blasques (2012). The three selected analytical approaches are evaluated with respect to accuracy of the cross-sectional results and the computation time. The best compromise ~~serve~~ serves as basis for the cross-sectional calculation module of the beam based design tool *PreDoCS* (Preliminary Design of Composite Structures).

2 Beam theories

A beam ~~as~~ is a mechanical model ~~is characterised by~~ of a structure that is characterized by a configuration where one geometric dimension ~~being significantly~~ is at least one order of magnitude larger than the other two. This allows the beam to be represented by two-dimensional cross-sections (formed by the shorter geometric dimensions) threaded along the beam axis (the longer geometric dimension). The calculation of the beam ~~, which is a three-dimensional problem, to be divided into a two-dimensional cross-section calculation and a one-dimensional beam calculation~~ is thus subdivided into the 2D calculation of cross-sectional properties and a line-like calculation of the beam (often referred to as 1D analysis), the axis of which being potentially curvilinear in space. This procedure is also called dimensional reduction (Hodges, 2006) and is described in the following subsections.

2.1 Recovery relations between beam and cross-section

The first step is to set up ~~an approach for~~ the kinematic relations ~~of a cross-section, for which the displacements at~~ that link the displacements in each point of a cross-section ~~can be calculated from the beam displacements at this point (~~to the displacements and rotations, or curvatures, of the beam at the respective axial position. These relations are also called "recovery relations"~~)~~. The formulation of the cross-sectional displacements is the core of the cross-sectional theory. From these, the cross-sectional strains are calculated as the derivatives of the displacements. In a second step, the constitutive relations of the material (material stiffness) ~~is~~ are used to calculate the ~~cross-sectional stress distribution~~ stress distribution in the cross-section from the strains. The cross-sectional stiffness matrix is derived ~~with~~ using the principle of virtual work. The spatial integration of the stress and strain ~~distribution describes the~~ distributions across the cross-section yields the internal loads (cutting forces ~~) of a~~ and moments) acting on the respective cross-section. Substituting the stresses and strains by the kinematic and the constitutive equations of the material results in the relation between the displacements and the internal loads of the cross-section which ~~denotes~~ forms the cross-sectional stiffness matrix.

2.2 ~~1D-FE-Beam~~Finite Beam Element Model

In case of simple load cases (defined by loads and boundary conditions) ~~for beams with only one~~ and beams with a constant cross-section, the displacements along the beam can be calculated analytically. For more complex load cases ~~, the 1D-FE beam model,~~ and geometries, a finite beam element model using the cross-sectional ~~stiffnesses~~ stiffness matrices from above, ~~has to be solved which results in the displacements of the entire beam. Now the~~ needs to be employed. Solving the finite element problem yields the displacements and rotations along the beam. The recovery relations from the previous subsection can then be used to ~~obtain~~ calculate the cross-sectional displacements at each point ~~of~~ along the beam. ~~From then, the~~ The strain and stress ~~distribution are~~ distributions are subsequently calculated according to the cross-sectional theory as described in the previous subsection ~~Hodges (2006)~~(Hodges, 2006).

2.3 Degrees of freedom of a cross-section

In general, the cross-sectional stiffness ~~relation~~ relations of a beam ~~can be written as follows~~ are given by the expression

$$\boldsymbol{F} = \boldsymbol{K}\boldsymbol{q}, \tag{1}$$

where $\boldsymbol{K}$ is the cross-sectional stiffness matrix, $\boldsymbol{q}$ is the vector of cross-sectional displacements and $\boldsymbol{F}$ is the vector of the cross-sectional internal loads according to the notation of Jung and Nagaraj (2002). For simplicity, a notation of partial derivatives with subscripts are used, i. e. $\frac{\partial f}{\partial x} = f_{,x}$. ~~Like~~ As described by Hodges (2006), ~~depending on the theory, the cross-section has different~~ the cross-sectional degrees of freedom (DOF) ~~, thus~~ depend on the theory. Thus, the dimensions of $\boldsymbol{q}$ ~~and~~ , $\boldsymbol{F}$ ~~have also a different size~~ , and $\boldsymbol{K}$ ~~a different dimension. The DOF are defined with the~~ also depend on the theory used. The local

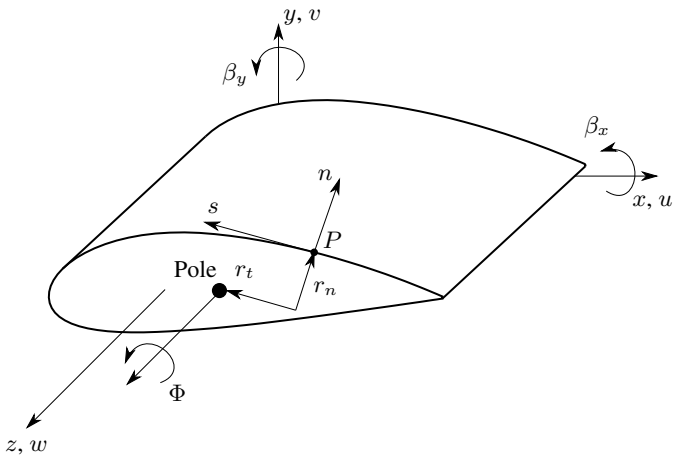

Figure 1. Global and contour coordinate system of the beam and cross-section displacements.

coordinate system and the DOF are shown in fig. 1. The longitudinal direction of the beam is denoted by the z-axis~~as beam-axis and the~~, and the cross-sectional plane is spanned by the x ~~-~~and y ~~-plane as cross-section as shown in fig. 1~~axes, respectively.

In case that only DOF for bending and extension are considered, the Euler-Bernoulli beam ~~model is the simplest and most common~~theory is employed. It has three cross-sectional DOF~~:~~, which are namely the longitudinal strain $w_{0,z}$ and the derivative of the ~~twist~~ rotation about the two axes ~~lying in the cross-section~~ parallel to the cross-sectional plane, $\beta_{x,z}$ and $\beta_{y,z}$. ~~Thus~~ Hence, $\boldsymbol{q}$ has ~~a length of 3~~ 3 entries and $\boldsymbol{K}$ ~~a size of~~ is of order 3×3. In order to consider ~~the~~ shear deformation, the Timoshenko beam theory can be used~~(a~~, which is also referred to as first order shear deformation theory ~~,~~ (FSDT). The cross-section has ~~then two more DOF :~~ two additional DOF in this case, which are the shear deformation angle in the x-z-plane γ_{xz} and the shear deformation angle in the y-z-plane γ_{yz}. ~~Thus~~ The vector of cross-sectional displacements $\boldsymbol{q}$ ~~has a length of 5~~ is then extended to 5 entries and $\boldsymbol{K}$ ~~a size of~~ is of order 5×5. In addition, the extension~~and bendingpart of the theory~~, bending, and shear parts can be supplemented by a ~~torsional part. The corresponding DOF of the torsional theory are added to the existing ones~~contribution from torsion by including the respective DOF. St. Venant ~~'s~~ theory adds one additional DOF~~(the twist~~, which is the derivative of the elastic twist angle around the beam axis denoted by $\phi_{,z}$~~), Vlasov 's theory would add two additional DOF(the twist $\phi_{,z}$ and the~~. Vlasov theory additionally adds one DOF, namely the restrained warping of the cross-section which is a function of the second derivative of the ~~twist~~ elastic twist angle denoted by $\phi_{,zz}$~~). Different~~.

As described above, different cross-section theories ~~use~~ employ different numbers of DOF~~as~~, which is also shown in table 1. For example, the approach of Jung (line 5 in table 1) uses a combination of Timoshenko and ~~Vlasovs Theory~~ Vlasov theories which results in a stiffness matrix $\boldsymbol{K}$ of ~~size~~ order 7×7, as further described in section 2.6.

2.4 Cross-sectional calculation approaches and their properties

An extensive comparison of cross-sectional theories based on ~~requirements, specifically derived for the design of rotor blades,~~ rotor blade-specific requirements has been carried out~~and an extract of this~~ . An excerpt is shown in table 1. Since different assumptions are made~~for each approach, different effects can be represented. Therefore, based on the described requirements~~ , the approaches show different abilities and limitations. Based on the requirements described in section 1, the following criteria were ~~selected to compare the approaches~~ chosen for comparing the approaches listed in table 1:

- ~~Cross-sectional geometry: open~~ Types of considered cross-sectional geometries: Open cross-sections, closed single-cell cross-sections, closed multi-cell cross-sections, ~~full~~ solid cross-sections, thin-walled contour, thick-walled contour
- ~~Calculation approach: analytical approach, 1D-FEM-approach, 2D-FEM-approach~~ General calculation approach: Analytical approach, 1D FE approach, 2D FE approach
- Considered effects:
  - Cross-sectional stiffness: Number of ~~DOF of a cross-section (~~cross-sectional DOF (i. e., dimension of the stiffness matrix), ~~Elastic~~ elastic coupling of the individual ~~DOF of the cross-section, Displacement~~ cross-sectional DOF, displacements due to shear ~~force (shear-soft model~~forces (i. e., shear-deformable theory)
  - Effects due to restrained warping (e.g., occurrence of warping normal stresses)
  - In-plane cross-sectional deformations (e.g., due to transverse contraction)
  - Out-of-plane cross-sectional deformations (e.g., warping due to torsion)
- Material behaviour:
  - Modelling as a disc: constant stresses over the contour thickness
  - Modelling as a plate: non-constant stresses over the contour thickness
  - Consideration of transverse shear (shear in contour thickness direction)
- ~~Force flow~~ Zero force flux in contour direction (circumferential stresses~~) are equal to zero (~~, common assumptions, not usable for structures under internal pressure, restrained deformation in circumferential direction not considered)
- Linear longitudinal strain distribution over the cross-section ~~, ~~(corresponds to the assumptions of the beam models according to Euler-Bernoulli and Timoshenko)

The cross-sectional approaches ~~of~~ in table 1 can be categorized in different ways. One possibility is the method ~~how the~~ for the calculation of the cross-sectional stiffness~~is calculated~~.

There are ~~2D FE approaches , which build up the cross-section~~ approaches that calculate the cross-sectional stiffness from two-dimensional finite element models (Blasques, 2012; Hodges, 2006; Yu, 2007), ~~as well as a mixture of analytical and FE~~

Table 1. Comparison of existing approaches for the cross-sectional calculation of composite beams

Reference	Open CS	Closed one-cell CS	Closed multi-cell CS	Thin-walled CS	Thick-walled CS	Solid CS	Calculation approach	Dimension of the stiffness matrix	Elastic couplings	Shear-soft model	Out-of-plane deformation	In-plane deformation	Restrained warping	Disc model	Plate model	Transverse shear in constitutive relations	No circumferential stresses	Linear longitudinal strain distribution	Comments
Wiedemann (2007)	-	x	x	x	-	-	Analytic	4	-	-	x	-	-	x	x	-	x	-	Only for isotropic materials
Chandra and Chopra (1992)	x	x	x	x	-	-	Analytic	9	x	x	x	-	x	x	x	-	x	-	Extension for multi-cell CS
Dugas (2002)	-	x	-	x	-	-	Analytic	4	x	-	-	-	-	x	-	-	x	x	Simple approach
Johnson et al. (2001)	-	x	-	x	-	-	Analytic	6	x	x	-	-	-	x	-	-	x	x	Force-based formulation
Jung et al. (2002)	x	x	x	x	x	-	Analytic	7	x	x	x	-	x	x	x	x	x	-	Mixed formulation for thick-walled CS
Kim and White (1997)	-	x	-	x	x	-	Analytic	6	x	x	x	-	-	x	-	x	x	-	Only rectangular CS
Libove (1988)	-	x	x	x	-	-	Analytic	-	x	x	-	-	-	x	-	-	x	x	Comparable to Mansfield and Sobey (1979)
Mansfield and Sobey (1979)	-	x	-	x	-	-	Analytic	4	x	-	-	-		x	-	-	x	x	
Qin and Librescu (2002)	-	x	-	x	-	-	Analytic	7	x	x	x	-	x	x	x	x	x	-	Comparable to Chandra and Chopra (1992), but with transverse shear and 7x7-stiffness matrix
Rehfield et al. (1990)	-	x	-	x	-	-	Analytic	7	x	x	x	-	-	x	-	-	x	-	Usage of a torsional warping function
Weisshaar (1978)	-	x	-	x	-	-	Analytic	2	x	-	-	-	-	x	-	-	x	x	Only bending around one axis and torsion
Vo and Lee (2008)	-	x	-	x	-	-	Analytic	8	x	x	x	-	x	x	-	x	x	-	Extension of Lee (2005) for closed cross-sections
Librescu and Song (1991)	-	x	-	x	-	-	Analytic	7	x	x	x	-	x	x	x	x	x	-	
Song (1990)	x	x	x	x	-	-	Analytic	7	x	x	x	-	x	x	x	x	x	-	~~Comprehensive presentation, taking into account primary and secondary~~ Taking into account prim. and second. warping
Suresh and Nagaraj (1996)	-	x	-	x	-	-	Analytic	7	x	x	-	-	x	x	-	-	x	x	Extension of Rehfield et al. (1990)
Kollár and Springer (2003)	x	x	x	x	x	x	Analytic	7	-	x	x	-	x	x	x	x	x	-	
Deo and Yu (2020)	-	x	x	x	x	-	1D FEM	4	x	-	x	-	-	x	x	-	x	-	
Saravia et al. (2015); Saravia (2016)	-	x	x	x	-	-	1D FEM	6	x	x	x	-	-	x	-	-	x	-	Warping function with 1D-FE-approach, remaining part is analytical
Carrera and Petrolo (2011)	x	x	x	x	x	x	2D FEM	6	x	x	x	x	-	x	x	-	-	-	Only for isotropic materials
Giavotto et al. (1983)	x	x	x	x	x	x	2D FEM	6	x	x	x	x	-	x	x	x	-	-	BECAS ~~Blasques (2012)~~ (Blasques, 2012), Extension for pre-bended and pre-twisted beams ~~Borri et al. (1992)~~ (Borri et al., 1992)
Hodges (2006)	x	x	x	x	x	x	2D FEM	6	x	x	x	x	-	x	x	x	-	-	Variational Asymptotic Method (VAM)
Yu et al. (2005)	x	-	-	x	x	-	2D FEM	5	x	-	x	x	-	x	x	-	-	-	Generalized Vlasov theory (VABS incl. warping)

approachesor approaches that combine analytical procedures and FE models. For the mixed case, an analytical approach is derived to calculate the cross-sectional stiffness, but with the warping of the cross-section assumed as given . This warping is then determined in the second step with a 1D-FE assuming given cross-sectional warping. The warping is subsequently determined with a 1D FE model over the thin-walled contour (cf. Saravia et al., 2015).

The analytical approaches (see table 1, column "calculation approach") can be divided into two categories, the displacement-based formulation and the force-based formulation Jung et al. (2002) which (Jung et al., 2002). They differ in the calculation of the shear stresses. The displacement-based formulation, which is also called stiffness method, has been used e. g. by Rehfield et al. (1990), Song (1990), Chandra and Chopra (1992) and Wiedemann (2007). A displacement field of the cross-section is assumed, from which the shear stresses can then be calculated directly with the help of the using the constitutive relations. The force-based formulation also assumes cross-sectional displacements and a normal stress distribution is calculated using constitutive relations. Based on the normal stress distribution, the shear stresses are calculated with the help of the by integration of the equilibrium condition on a contour element (cf. Jung et al., 2002). The force-based formulation thus leads to better shear stress distributions (Johnson et al., 2001). This approach was used e. g. by Mansfield and Sobey (1979), Libove (1988), and more recently for thin-walled composite beams by Johnson et al. (2001), see table 1. A combination of the displacement- and force based force-based formulation was introduced by Jung and Nagaraj (2002) and is further explained in section 2.6.

2.5 Selected approaches based on requirements of for wind turbine blades

Based on the requirements described in section 1 and the available approaches listed in table 1, three different approaches were selected. An FE-approach FE-based approach was already excluded due to the high computational cost which will also be shown in section 3.4. From the analytical approaches which fulfill Five analytical approaches fulfilling the multi-cell criterion are available (see table 1)only five approaches remain. The approach of Libove (1988) do not deliver does not provide a cross-sectional stiffness matrix. Chandra and Chopra (1992) take into account additional DOF for the derivation of the shear forces which correspond to the line loads. These additional DOF make the approach more complexand , but are not required for the intended application. The first selected approach for an implementation is the one of Wiedemann (2007)approach selected for implementation is that of Wiedemann (2007), which includes a shear-stiff formulation based on a 3×3 stiffness matrix(and . It comprises a torsional stiffness) without , but neglects bend-twist coupling- coupling and shear stiffness terms. Therefore, it does not fulfill all requirements given in section 1but is chosen anyway , but is nevertheless chosen due to its fastness and simplicity for implementation. To fulfill the simplicity and the resulting short computation times. The second approach selected for implementation is the displacement-based formulation of Song (1990), which fulfills the requirements with respect to the elastic coupling and shear stiffness terms , the displacement-based formulation of Song (1990) was chosen as the second approach. It includes furthermore and further includes transverse shear and also restrained warping(restrained warping, resulting in a 7×7 stiffness matrix). As a third approach the mixed-formulation . The third approach is the mixed formulation (displacement- and force basedforce-based) of Jung and Nagaraj (2002)was chosen due to the expectation , as it was expected that it best fulfills the derived requirements and delivers probably requirements and probably yields better results in comparison to Song (1990). The three methods are implemented as “Wiedemann”, “Song” and “Jung” -approach in

approaches in the in-house code *PreDoCS* to create and compare cross-section stiffness matrices and stress distributions. In the following section, the theory of the "Jung"-approach is ~~presented.~~ discussed in more detail, as it is representative for the other two approaches as well. The derivation of the other analytical approaches can be found in the original literature.

2.6 Theoretical treatment of ~~-approach~~the "Jung" approach

The ~~cross-section theory which is used in PreDoCS as~~ cross-sectional theory named "Jung" ~~-approach is derived~~ approach as described by Jung and Nagaraj (2002) ~~. The theoretical treatment is presented~~ is reviewed in the following~~, to understand the general approach of determining the cross-sectional stiffness matrix based on the example of the -approach~~. The derived cross-sectional stiffness matrix is required for the comparison ~~to~~ with the other cross-sectional approaches conducted in section 3.

~~Jung's~~ The "Jung" approach is a so-called mixed approach, or semi-inverse approach~~, because~~ . Therein, all element stresses except ~~of~~ the shear stress and the hoop moment can be directly calculated with the given ~~cross-section~~ cross-sectional displacements. The shear stress and the hoop moment are treated as unknowns and are determined by using continuity conditions around each cell of the cross-section.

2.6.1 Kinematics

~~Contrary~~ In contrast to Jung and Nagaraj (2002), the z-axis is used as the beam axis, ~~not the x-axis~~see also fig. 1. This leads to different kinematic equations ~~which~~ that are adopted from Librescu (2006). Additionally, the ~~direction of the~~ moment around the y ~~-axis (~~axis (which is the z ~~-axis~~ axis in the Jung coordinate system) is defined ~~the opposite way round~~positive in the opposite direction. Figure 1 shows the ~~two used coordinate systems~~ coordinate systems used. These are an orthogonal Cartesian coordinate system (x, y, z) and a curvilinear coordinate system (n, s, z) at the point P, where s is measured along the ~~middle surface~~ mid-surface of the shell wall and n is normal to s. The pole is the pole of rotation ~~around the z-axis~~ of the cross-section around the z axis and is assumed ~~as~~ given for the derivation of the kinematics.

~~Assumptions are made for the strains (ϵ_{zz}~~The strains of the contour (ε_{zz}, κ_{zz}, κ_{zs}) ~~of the contour dependent on the cross-section~~ can be fomulated as functions of the cross-sectional displacements ($w_{p,z}$, $\beta_{x,z}$, $\beta_{y,z}$, $\phi_{,z}$, $\phi_{,zz}$, γ_{xz}, γ_{yz})~~:~~ , which are given by the relationships

$$
\begin{aligned}
\epsilon\varepsilon_{zz} &= w_{p,z}(z) - x(s)\cdot\beta_{y,z}(z) + y(s)\cdot\beta_{x,z}(z) - \omega(s)\cdot\phi_{,zz}(z),\\
\kappa_{zz} &= -\beta_{x,z}(z)\cdot x_{,s}(s) - \beta_{y,z}(z)\cdot y_{,s}(s) + r_t(s)\cdot\phi_{,zz}(z),\\
\kappa_{zs} &= 2\cdot\phi_{,z}(z).
\end{aligned}
\tag{2}
$$

2.6.2 Constitutive Relations

To describe the material behavior~~the CLT (~~, the classical laminate theory (CLT) is used with the complete and coupled 6x6 disc and plate stiffness matrix ~~. Furthermore, the~~ of the shell (also referred to as ABD matrix). The transverse shear stiffness of the plate is also considered. The force and moment ~~flows~~ fluxes on an infinitesimal piece of the shell are shown in fig. 2.

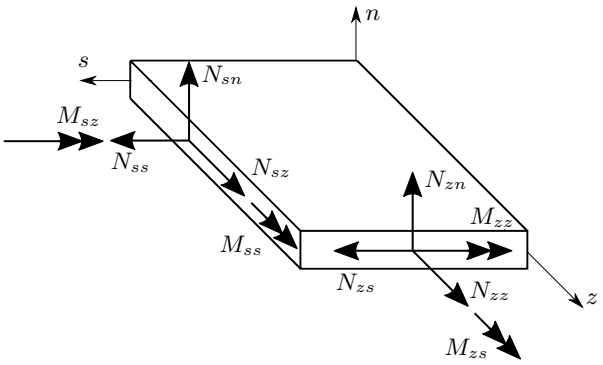

Figure 2. Shell forces and moments based on Jung and Nagaraj (2002).

The constitutive relations are semi-inverted to obtain the missing force and moment ~~flows and strains~~ fluxes (N_{zz}, M_{zz}, M_{zs}~~,~~) and strains (γ_{zs}, κ_{ss}) from the strains and ~~flows~~ fluxes for which assumptions are ~~given~~ made (displacement-based part: ~~ϵ_{zz}~~ε_{zz}, κ_{zz}, κ_{zs}; force-based part: N_{zs}, M_{ss}). ~~It follows for~~ For the constitutive relations~~:~~, it follows that

$$\begin{pmatrix} N_{zz} \\ M_{zz} \\ M_{zs} \\ \gamma_{zs} \\ \kappa_{ss} \end{pmatrix} = \boldsymbol{C} \cdot \begin{pmatrix} \varepsilon_{zz} \\ \kappa_{zz} \\ \kappa_{zs} \\ N_{zs} \\ M_{ss} \end{pmatrix}. \tag{3}$$

2.6.3 Determination of N_{zs} and M_{ss}

~~An assumption~~ Assumption for N_{zs} and M_{ss} ~~is~~ are made in (Jung and Park, 2005, eq. 13, force-based approach)~~:~~. They are given by the expressions

$$N_{zs} = N_{zs}^0 - \int_0^s N_{zz,z}\, ds, \tag{4}$$

$$M_{ss} = M_{ss}^0 + x M_{ss}^x + y M_{ss}^y - \int_0^s M_{zs,z}\, ds, \tag{5}$$

where N_{zs}^0 , M_{ss}^0 , M_{ss}^x , and M_{ss}^y represent the unknown circuit shear ~~flows~~ fluxes and hoop moments for each cell of a closed multi-cell section.

To obtain the continuity condition for each cell of the multi-cell cross-section, four conditions for each cell (C_i) are used that are given by

$$\oint_{C_i} \gamma_{zs}\, ds = 2A_i \cdot \phi_{,z}, \tag{6}$$

$$\oint_{C_i} \kappa_{ss}\, ds = 0, \tag{7}$$

$$\oint_{C_i} x \cdot \kappa_{ss}\, ds = 0, \tag{8}$$

$$\oint_{C_i} y \cdot \kappa_{ss}\, ds = 0,0. \tag{9}$$

~~where~~ Herein, A_i is the enclosed area of the respective cell i.

After solving this linear ~~equation system~~ system of equations for the given cross-sectional geometry, the variables N^0_{zs}, M^0_{ss}, M^x_{ss} and M^y_{ss} are ~~given and the following relationship arises:~~ obtained yielding an expression for N_{zs} and M_{ss} given by

$$\begin{pmatrix} N_{zs} \\ M_{ss} \end{pmatrix} = \boldsymbol{\xi} = \boldsymbol{\xi}^a + \boldsymbol{\xi}^r = \boldsymbol{f} \cdot \boldsymbol{q}_b + \boldsymbol{F} \cdot \boldsymbol{q}_{b,z}, \tag{10}$$

~~with $\boldsymbol{q_b} = \begin{pmatrix} w_{p,z} & \beta_{x,z} & \beta_{y,z} & \phi_{,z} & \phi_{,zz} \end{pmatrix}^T$ and $\boldsymbol{\xi^a}$ and $\boldsymbol{\xi^r}$ as~~ where $\boldsymbol{q}_b = \begin{pmatrix} w_{p,z} & \beta_{x,z} & \beta_{y,z} & \phi_{,z} & \phi_{,zz} \end{pmatrix}^T$ and $\boldsymbol{\xi}^a$ and $\boldsymbol{\xi}^r$ are the active and reactive parts of the shear ~~flow~~ flux and hoop moment ~~according to the definition of~~ as defined by Gjelsvik and Hodges (1982).

2.6.4 Cross-Sectional Stiffness Relations

The cross-sectional stiffness relations are ~~determined in two steps, first the active part~~ subdivided into an active part (denoted by $\boldsymbol{K}_{bb}$) and a reactive part (denoted by $\boldsymbol{K}_{vv}$ and ~~afterwards the reactive part .~~

~~**Active part ($\boldsymbol{K_{bb}}$)**~~

~~In order to determine the cross-sectional stiffness matrix in the first step, only the~~ $\boldsymbol{K}_{bv}$), which are derived in the following. The active part of the strain energy is considered ~~. With~~ first. Using the principle of virtual work, the active strain energy related to the virtual strains ~~results in~~ becomes

$$W_a = \int_C \left(N_{zz} \cdot \delta\varepsilon_{zz} + M_{zz} \cdot \delta\kappa_{zz} + M_{zs} \cdot \delta\kappa_{zs} + N_{zs} \cdot \delta\gamma_{zs} + M_{ss} \cdot \delta\kappa_{ss}\right) ds. \tag{11}$$

Herein, the virtual strains are derived from the virtual ~~cross-section displacements $\delta\boldsymbol{q_b}$~~ cross-sectional displacements $\delta\boldsymbol{q}_b$. With the help of equation eq. (11), it is possible to establish a relation between the ~~cross-section displacements $\boldsymbol{q_b}$~~ cross-sectional displacements $\boldsymbol{q}_b$ and the corresponding ~~cross-section~~ cross-sectional loads given by

$$\boldsymbol{F}_b = \begin{pmatrix} N & M_x & M_y & T & M_\omega \end{pmatrix}^T = \boldsymbol{K}_{bb} \cdot \boldsymbol{q}_b, \tag{12}$$

where N is the normal force, M_x and M_y are the bending moments around the x ~~- and~~ and the y ~~-axis~~axis, respectively, T is the torsion moment, and M_ω is the warping bi-moment.

~~**Reactive part ($\boldsymbol{K}_{vv}$ and $\boldsymbol{K}_{bv}$)**~~

In order to obtain the shear stiffness terms, a cantilevered beam is considered that is loaded at the tip ~~with shear forces~~ by shear forces in the x direction, V_x ~~and~~ , and the y direction, V_y ~~is considered. Differentiating $\boldsymbol{F}_b$~~ , following the first-order shear deformation theory. It has to be noted that this case does not represent the wind turbine blade use-case. Once the stiffness and mass properties of all cross-sections are calculated, a beam model consisting of several different cross-sections representing the blade certainly needs to be constructed and can subsequently be used to carry out loads simulations, obtaining the real load distribution along the blade. Differentiating the cross-sectional load vector $\boldsymbol{F}_b$ with respect to z ~~, the following equation can be obtained by~~ yields the expression

$$_{,z}\boldsymbol{F}_{b,z} = \begin{pmatrix} 0 & -V_y & V_x & 0 & 0 \end{pmatrix}^T = \boldsymbol{K}_{bb} \cdot {}_{,z}\boldsymbol{q}_{b,z}. \tag{13}$$

With ~~$\boldsymbol{q}_{b,z} = \boldsymbol{K}_{bb}^{-1} \cdot \boldsymbol{F}_{b,z}$, the cross-section~~ $\boldsymbol{q}_{b,z} = \boldsymbol{K}_{bb}^{-1} \cdot \boldsymbol{F}_{b,z}$ denoting the cross-sectional displacements for extension, bending and torsion, the reactive part of the shear ~~flow $\boldsymbol{\xi}^r$~~ flux $\boldsymbol{\xi}^r$ can be determined using

$$\boldsymbol{\xi}^r = \boldsymbol{F} \cdot \boldsymbol{K}_{bb}^{-1} \cdot \begin{pmatrix} V_x \\ V_y \end{pmatrix} = \boldsymbol{f}^r \cdot \begin{pmatrix} V_x \\ V_y \end{pmatrix}. \tag{14}$$

The shear forces are calculated with the matrix $\boldsymbol{p}$, which is defined by

$$\begin{pmatrix} V_x \\ V_y \end{pmatrix} = \boldsymbol{p} \cdot \boldsymbol{q}. \tag{15}$$

Herein~~is~~ , $\boldsymbol{q} = \begin{pmatrix} w_{p,z} & \beta_{x,z} & \beta_{y,z} & \phi_{,z} & \phi_{,zz} & \gamma_{xz} & \gamma_{yz} \end{pmatrix}^T$ is the complete vector of the cross-sectional displacements. The matrix $\boldsymbol{p}$ is splited in a 2x5 left part called $\boldsymbol{p}_1$ and a 2x2 right part called $\boldsymbol{p}_2$.

~~**Full cross-section stiffness matrix**~~

Introducing

$$\boldsymbol{K}_{vv} = \boldsymbol{f}^{rT} \cdot \boldsymbol{\Lambda} \cdot \boldsymbol{f}^{rT} \tag{16}$$

Table 2. Explanation of the indices of the cross-section stiffness matrix $\boldsymbol{K}$, the cross-section displacements $\boldsymbol{q}$, and the internal loads $\boldsymbol{F}$.

Index	Internal load type
1	Transversal force in x-direction
2	Transversal force in y-direction
3	Extension
4	Bending around the x-axis
5	Bending around the y-axis
6	Torsion
7	Warping

and

$$\boldsymbol{K}_{bv} = \boldsymbol{f}^T \cdot \boldsymbol{\Lambda} \cdot \boldsymbol{f}^{r\,T}, \tag{17}$$

with $\boldsymbol{\Lambda} = \begin{bmatrix} C_{44} & C_{45} \\ C_{45} & C_{55}, \end{bmatrix}$, the resulting 7x7 ~~cross-section~~ cross-sectional stiffness matrix $\boldsymbol{K}$ is obtained~~. It~~, which is given by the expression

$$\boldsymbol{K} = \begin{bmatrix} \left[\boldsymbol{K}_{bb} + 2\boldsymbol{K}_{bv}\boldsymbol{p}_1 + \boldsymbol{p}_1^T \boldsymbol{K}_{vv}\boldsymbol{p}_1\right] & \left[\boldsymbol{K}_{bv}\boldsymbol{p}_2 + \boldsymbol{p}_1^T \boldsymbol{K}_{vv}\boldsymbol{p}_2\right] \\ \left[\boldsymbol{K}_{bv}\boldsymbol{p}_2 + \boldsymbol{p}_1^T \boldsymbol{K}_{vv}\boldsymbol{p}_2\right] & \left[\boldsymbol{p}_2^T \boldsymbol{K}_{vv}\boldsymbol{p}_2\right] \end{bmatrix}. \tag{18}$$

Substitution into eq. (1) yields the relationship between the ~~cross-section~~ cross-sectional displacements $\boldsymbol{q}$ and the internal loads $\boldsymbol{F}$. The order of both vectors is given in table 2.

It should be mentioned that ~~due to the approach for the kinematics , the point of application~~ the formulation of the kinematics results in a point of attack for extension and bending loads ~~is~~ that is located in the origin of the cross-section coordinate system. The point of ~~application~~ attack for transversal and torsion loads is the pole (also referred to as shear center), see fig. 3.

3 Comparison of cross-sectional approaches

In this section, the mechanical properties for six different test cases (with two different cross-section geometries) are determined ~~with the help of the~~ utilizing the three cross-sectional approaches selected in section 2.5. Thereby, the stiffness matrix, the positions of the ~~elastic-~~ elastic and the shear center, and the stress ~~distribution~~ distributions across the cross-section are compared ~~. The~~ with the results of the ~~2D-FE cross-section~~ 2D FE solver BECAS (Blasques, 2012)~~serves as reference.~~ , which serves as a reference. The elastic center is the point where an axial force does not induce bending. The shear center is the point where applied transverse forces do not induce torsional twist. The presented analytical approaches use the origin of the cross-section as application point for axial forces and bending moments. The transverse forces and torsional moments are

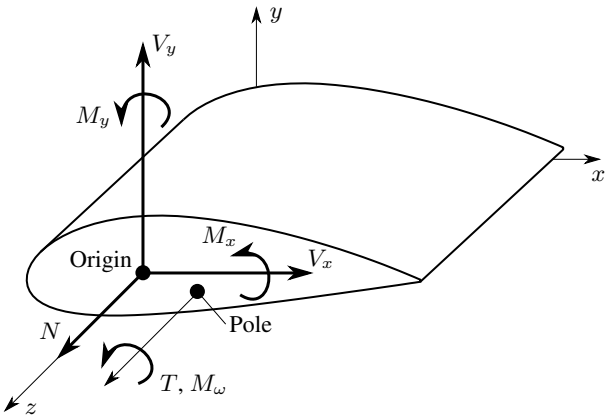

Figure 3. Points of attack for the internal loads.

applied at the shear center. Both analytical approaches, Song and Jung, require the pole (center of rotation of the cross-section) as input for the kinematic formulations. With the assumption that the center of rotation equals the shear center, the Wiedemann (2007) approach is the only approach that can be used to determine the shear center in advance. In contrast to the analytical approaches, the application point for all force and moment load of the cross-section for BECAS is the origin. To be able to compare the analytical approaches with BECAS, the origin of the cross-section must coincide with the shear center. This is achieved by translating the cross-section geometry accordingly prior to the analysis. In case of Song and Jung the shear center ~~is determined based on~~ can be obtained from the shear stress distribution, as the shear center can also be referred to as the point of attack of the resultant shear force.

3.1 Test cases

The comparison is carried out using two different cross-sections with different material distributions. One cross-section ~~as~~ is a thin-walled rectangle (~~??~~fig. 4a), allowing a visual verification of ~~expecting~~ expected stress distributions for simple load cases. The second cross-section is a NACA 2412 airfoil with two shear webs at 30 % and 50 % ~~chord shown in ??, which~~ of the chord length, measured from the leading edge, as shown in fig. 4b. This cross-section is representative for a ~~cross-section of a~~ wind turbine rotor blade. For the distinction between effects caused by the geometry ~~and~~ or the material, two material concepts are used: Aluminum as an isotropic material ($E = 71 \times 10^3\,\mathrm{MPa}$, $\nu = 0.32$) and a composite layup ~~, made up of a~~ consisting of carbon fibre UD prepreg based on Hexcel T800/M21 ($E_1 = 134.7 \times 10^3\,\mathrm{MPa}$, $E_2 = 7.7 \times 10^3\,\mathrm{MPa}$, $\nu_{12} = 0.369$, $\nu_{22} = 0.5$, $G_{21} = 4.2 \times 10^3\,\mathrm{MPa}$, $t = 0.184\,\mathrm{mm}$). The stacking sequence of the webs of the NACA 2412 airfoil is $(0/45_2/-45_2/90_2/45_2/-45_2/0)_s$, all other stacking sequences are $(0_2/45/0_2/-45/0_2/45/90/-45/90)_s$. Based on the two cross-sections and the ~~afore mentioned materials~~aforementioned materials, the following test cases are created and assigned a unique ID:

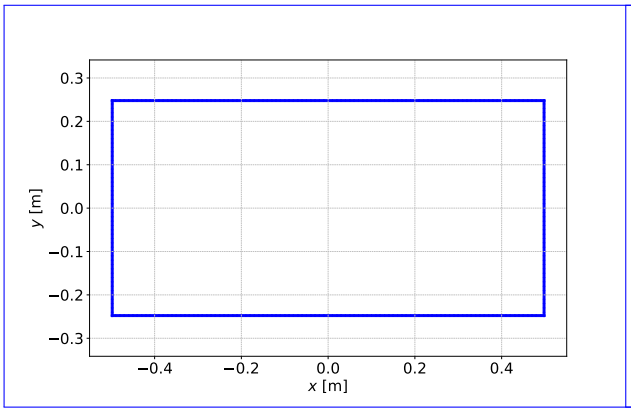

(a) Test cases ~~900-903~~0-3 (PreDoCS).

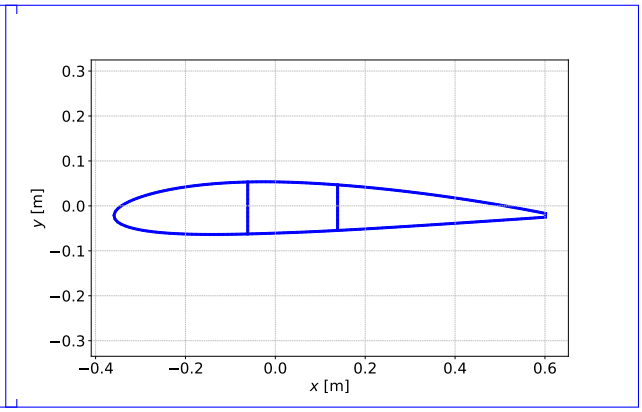

(b) Test cases ~~910~~ 10 and ~~911.~~11 (PreDoCS).

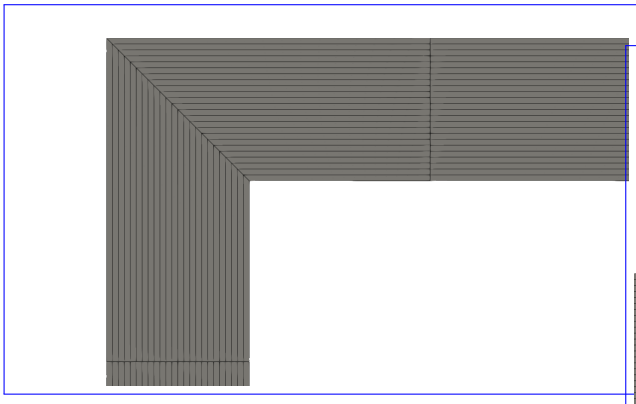

(c) ~~Cross-section geometries~~ Test cases 1-3 (~~nodes as black circles~~BECAS), ~~elements as blue lines~~close-up of the left upper corner.

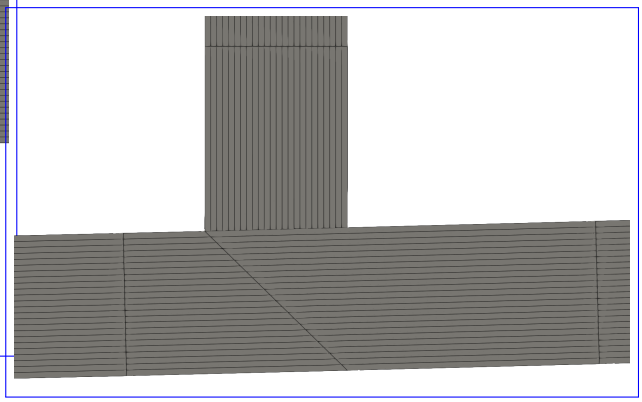

(d) Test case 11 (BECAS), close-up of the front lower web-shell-intersection.

Figure 4. Cross-section geometries (top) and BECAS mesh of geometric details (below).

- ~~900: Rect. 0: Rectangular~~ CS made of ~~2 mm aluminum sheets~~ 4.416 mm aluminum (same thickness as the composite layup)
- ~~901: Rect. 1: Rectangular~~ CS made of the composite layup described above
- ~~902: Rect. 2: Rectangular~~ CS made of the composite layup described above rotated by 30° ~~, walls opposite to each other with different sign to~~ in all walls to get a Circumferentially ~~Asymmetric~~ Uniform Stiffness configuration ~~(CAS, Libresecu, 2006, p. 91)~~ (CUS, Librescu, 2006, p. 88)
- ~~903: Rect. 3: Rectangular~~ CS made of the composite layup described above rotated by 30° ~~in all walls to~~ , walls opposite to each other with different sign to get a Circumferentially ~~Uniform~~ Asymmetric Stiffness configuration ~~(CUS, Librescu, 2006, p. 88)~~ (CAS, Librescu, 2006, p. 91)

Table 3. Number of elements of the cross-sections for the different approaches.

Test case ID	Wiedemann, Song, Jung	BECAS
~~900~~ 0	~~30~~ 300	~~30~~ 300
~~901~~ 1	~~30~~ 300	~~30 · 24 = 720~~ 300 · 24 = 7200
~~902~~ 2	~~30~~ 300	~~30 · 24 = 720~~ 300 · 24 = 7200
~~903~~ 3	~~30~~ 300	~~30 · 24 = 720~~ 300 · 24 = 7200
~~910~~ 10	~~58~~ 225	~~58~~ 225
~~911~~ 11	~~58~~ 225	~~58 · 24 = 1392~~ 225 · 24 = 5400

- ~~910~~10: NACA 2412 CS made of ~~2 mm~~ 4.416 mm aluminum
- ~~911~~11: NACA 2412 CS made of the composite layups described above

To obtain accurate results for BECAS, a fine mesh and an accurate geometric representation of the cross-section is required (Maes et al., 2024). The contour is discretized in contour direction similarly for all cross-section calculations based on a mesh convergence study. The rectangular cross-section (~~900-903~~0-3) is discretized in contour direction with ~~30 equidistant elements , the~~ 300 equidistant elements of 10 mm length. It should be mentioned that for the rectangular cross-section the analytical approaches are independent of the discretization and already obtain accurate results with a discretization of four elements in contour direction. A further discretization refinement does not affect the calculation results. Nevertheless, in order to be able to compare element-wise stresses, the same discretization in contour direction was chosen for the analytical approaches and for BECAS. The airfoil with webs (~~910 and 911~~test cases 10 and 11) is discretized in contour direction with ~~58 elements distributed according to the degree of the curvature~~225 elements of 10 mm length. The analytical approaches do not need a discretization in ~~contour-thickness-direction, BECAS reqiures~~ contour thickness direction, BECAS requires a discretization for each layer of the laminate in ~~contour-thickness-direction~~contour thickness direction. As the laminates consist of ~~24~~ 24 layers, 24 elements are used in thickness direction. The resulting number of elements for the different test cases and the different models are listed in table 3.

Table 4. Test case ~~901~~1, Rectangular cross-section with composite layup.

	BECAS	PreDoCS, Jung		PreDoCS, Song		PreDoCS, Wiedemann	
		value	diff. [%]	value	diff. [%]	value	diff. [%]
K_{11}	~~1.116×10^8~~	~~1.155×10^8~~	~~3.48~~ −0.16	~~1.399×10^8~~	~~25.30~~ 21.19	-	-
	1.152×10^8	1.150×10^8		1.396×10^8			
K_{22}	~~3.805×10^7~~	~~4.225×10^7~~	~~11.04~~ −0.49	~~9.055×10^7~~	~~137.96~~	-	-
	4.190×10^7	4.169×10^7		9.023×10^7	115.37		
K_{33}	~~9.689×10^8~~	~~1.045×10^9~~	~~7.82~~ 0.32	~~1.045×10^9~~	~~7.82~~ 0.32	~~1.045×10^9~~	~~7.82~~ 0.32
	1.038×10^9	1.042×10^9		1.042×10^9		1.042×10^9	
K_{44}	~~4.614×10^7~~	~~5.002×10^7~~	~~8.40~~ 0.41	~~5.002×10^7~~	~~8.40~~ 0.41	~~5.002×10^7~~	~~8.40~~ 0.41
	4.964×10^7	4.984×10^7		4.984×10^7		4.984×10^7	
K_{55}	~~1.281×10^8~~	~~1.443×10^8~~	~~12.64~~ 0.57	~~1.443×10^8~~	~~12.64~~ 0.57	~~1.443×10^8~~	~~12.64~~ 0.57
	1.428×10^8	1.436×10^8		1.436×10^8		1.436×10^8	
K_{66}	~~1.960×10^7~~	~~2.102×10^7~~	~~7.29~~ −0.49	~~2.102×10^7~~	~~7.28~~ −0.50	~~2.102×10^7~~	~~7.28~~ −0.50
	2.063×10^7	2.053×10^7		2.053×10^7		2.053×10^7	
K_{77}	-	~~6.047×10^5~~	-	~~6.047×10^5~~	-	-	-
		5.908×10^5		5.908×10^5			

3.2 Stiffness terms

The tables ~~??~~ 4-~~??~~ 7 show the non-zero values of the stiffness matrix and~~the elastic-~~ (, for the test case 11 (NACA 2412 profile), the positions of the elastic (EC) and shear centers (SC)~~of several test cases~~. The indices are according to the description given in table 2. ~~The shear stiffness terms of Song show high deviations compared to BECAS. In all test cases deviations above 20 % for K_{11} and between approximately 100 % and 300 % for K_{22} can be observed, due to the first-order shear deformation theory used by this approach. The Jung approach has deviations below 10 % which indicates a significant improvement. The Wiedemann approach does not cover the shear stiffness terms due to its shear-stiff formulation. The important coupling stiffness terms show a good accordance with the BECAS results. The stiffness term K_{36} for extension-torsion coupling of test case 902 (CAS) indicated a deviation of about 6 %. The stiffness terms K_{46} and K_{56} for bend-twist coupling of test case 903 (CUS) indicated a deviation of about 2 % to 3 %. Similar to the shear stiffness, the coupling terms are not present in the Wiedemann approach.~~

Table 5. Test case ~~9022~~, Rectangular cross-section with ~~CAS~~ CUS layup.

	BECAS	PreDoCS, Jung		PreDoCS, Song		PreDoCS, Wiedemann	
		value	diff. [%]	value	diff. [%]	value	diff. [%]
K_{11}	~~1.648×10^8~~ 1.706×10^8	~~1.723×10^8~~ 1.715×10^8	~~4.52~~ 0.49	~~2.024×10^8~~ 2.020×10^8	~~22.83~~ 18.39	-	-
K_{22}	~~5.628×10^7~~ 6.235×10^7	~~6.301×10^7~~ 6.217×10^7	~~11.95~~ −0.28	~~1.227×10^8~~ 1.223×10^8	~~118.06~~ 96.13	-	-
K_{33}	~~6.766×10^8~~ 7.256×10^8	~~7.300×10^8~~ 7.280×10^8	~~7.89~~ 0.32	~~7.300×10^8~~ 7.280×10^8	~~7.89~~ 0.32	~~7.300×10^8~~ 7.280×10^8	~~7.89~~ 0.32
K_{44}	~~3.227×10^7~~ 3.448×10^7	~~3.476×10^7~~ 3.464×10^7	~~7.70~~ 0.46	~~3.495×10^7~~ 3.483×10^7	~~8.30~~ 1.02	~~3.495×10^7~~ 3.483×10^7	~~8.30~~ 1.02
K_{55}	~~8.974×10^7~~ 9.968×10^7	~~1.008×10^8~~ 1.003×10^8	~~12.27~~ 0.58	~~1.008×10^8~~ 1.004×10^8	~~12.38~~ 0.67	~~1.008×10^8~~ 1.004×10^8	~~12.38~~ 0.67
K_{66}	~~2.894×10^7~~ 3.074×10^7	~~3.135×10^7~~ 3.062×10^7	~~8.33~~ −0.41	~~3.135×10^7~~ 3.062×10^7	~~8.32~~ −0.41	~~3.135×10^7~~ 3.062×10^7	~~8.32~~ −0.41
K_{77}	-	~~3.765×10^5~~ 3.679×10^5	-	~~4.225×10^5~~ 4.128×10^5	-	-	-
K_{14}	~~2.345×10^7~~ 2.464×10^7	~~2.494×10^7~~ 2.484×10^7	~~6.33~~ 0.82	~~2.474×10^7~~ 2.463×10^7	~~5.49~~ −0.03	-	-
K_{25}	~~2.299×10^7~~ 2.587×10^7	~~2.619×10^7~~ 2.595×10^7	~~13.93~~ 0.33	~~2.485×10^7~~ 2.463×10^7	~~8.10~~ −4.78	-	-
K_{36}	~~-4.569×10^7~~ -4.924×10^7	~~-4.992×10^7~~ -4.926×10^7	~~9.24~~ 0.04	~~-4.992×10^7~~ -4.926×10^7	~~9.24~~ 0.04	-	-

Table 6. Test case ~~9033~~, Rectangular cross-section with ~~CUS~~ CAS layup.

	BECAS	PreDoCS, Jung		PreDoCS, Song		PreDoCS, Wiedemann	
		value	diff. [%]	value	diff. [%]	value	diff. [%]
K_{11}	~~1.708×10^8~~ 1.692×10^8	~~1.723×10^8~~ 1.715×10^8	~~0.84~~ 1.33	~~2.024×10^8~~ 2.020×10^8	~~18.51~~ 19.38	-	-
K_{22}	~~6.147×10^7~~ 6.139×10^7	~~6.301×10^7~~ 6.217×10^7	~~2.50~~ 1.27	~~1.227×10^8~~ 1.223×10^8	~~99.66~~ 99.19	-	-
K_{33}	~~6.983×10^8~~ 7.111×10^8	~~7.168×10^8~~ 7.148×10^8	~~2.64~~ 0.52	~~7.300×10^8~~ 7.280×10^8	~~4.53~~ 2.38	~~7.300×10^8~~ 7.280×10^8	~~4.53~~ 2.38
K_{44}	~~3.265×10^7~~ 3.307×10^7	~~3.331×10^7~~ 3.320×10^7	~~2.04~~ 0.41	~~3.495×10^7~~ 3.483×10^7	~~7.05~~ 5.32	~~3.495×10^7~~ 3.483×10^7	~~7.05~~ 5.32
K_{55}	~~8.887×10^7~~ 9.106×10^7	~~9.206×10^7~~ 9.160×10^7	~~3.59~~ 0.59	~~1.008×10^8~~ 1.004×10^8	~~13.48~~ 10.20	~~1.008×10^8~~ 1.004×10^8	~~13.48~~ 10.20
K_{66}	~~3.064×10^7~~ 3.075×10^7	~~3.135×10^7~~ 3.062×10^7	~~2.32~~ −0.42	~~3.135×10^7~~ 3.062×10^7	~~2.32~~ −0.42	~~3.135×10^7~~ 3.062×10^7	~~2.32~~ −0.42
~~K_{77}~~ ~~3.874×10^5~~ ~~4.225×10^5~~ ~~K_{13}~~ K_{23}	~~-8.932×10^7~~ 8.940×10^7 ~~-3.107×10^7~~ -3.218×10^7	~~-9.143×10^7~~ 9.112×10^7 ~~-3.344×10^7~~ -3.313×10^7	~~2.36~~ 1.93 ~~7.63~~ 2.96	~~-9.983×10^7~~ 9.961×10^7 ~~-4.992×10^7~~ -4.970×10^7	~~11.77~~ 11.43 ~~60.65~~ 54.44	- -	- -
K_{45}	~~9.125×10^5~~ -2.177×10^6	~~2.179×10^6~~ -2.171×10^6	~~138.76~~ −0.25	0.000	−100.00	0.000	−100.00
K_{46}	~~8.005×10^6~~ -8.150×10^6	~~8.247×10^6~~ -8.144×10^6	~~3.02~~ −0.07	~~8.246×10^6~~ -8.144×10^6	~~3.01~~ −0.08	-	-
K_{56}	~~7.868×10^6~~ 8.140×10^6	~~8.283×10^6~~ 8.163×10^6	~~5.28~~ 0.29	~~8.283×10^6~~ 8.163×10^6	~~5.27~~ 0.28	-	-

Table 7. Test case ~~911~~11, NACA 2412 cross-section with composite layup.

	BECAS	PreDoCS, Jung		PreDoCS, Song		PreDoCS, Wiedemann	
		value	diff. [%]	value	diff. [%]	value	diff. [%]
x_{EC} [m]	~~0.131~~ 0.108	~~0.130~~ 0.109	~~−0.05~~ 0.06	~~0.130~~ 0.109	~~−0.05~~ 0.06	~~0.130~~ 0.109	~~−0.05~~ 0.06
y_{EC} [m]	~~−0.010~~ −0.009	~~−0.010~~ −0.009	~~−0.01~~ 0.00	~~−0.010~~ −0.009	~~−0.01~~ 0.00	~~−0.010~~ −0.009	~~−0.01~~ 0.00
x_{SC} [m]	~~0.005~~ 0.001	0.000	~~−0.49~~ −0.11	0.000	~~−0.49~~ −0.11	0.000	~~−0.49~~ −0.11
y_{SC} [m]	0.000	0.000	0.00	0.000	0.00	0.000	0.00
K_{11}	~~1.061×10^8~~ 1.018×10^8	~~1.056×10^8~~ 1.018×10^8	~~−0.43~~ −0.03	~~1.287×10^8~~ 1.240×10^8	~~21.40~~ 21.78	-	-
K_{22}	~~1.509×10^7~~ 1.526×10^7	~~1.547×10^7~~ 1.461×10^7	~~2.51~~ −4.22	~~5.582×10^7~~ 5.446×10^7	~~269.80~~ 256.93	-	-
K_{33}	~~7.454×10^8~~ 7.241×10^8	~~7.526×10^8~~ 7.270×10^8	~~0.97~~ 0.39	~~7.526×10^8~~ 7.270×10^8	~~0.97~~ 0.39	~~7.526×10^8~~ 7.270×10^8	~~0.97~~ 0.39
K_{44}	~~1.409×10^6~~ 1.389×10^6	~~1.408×10^6~~ 1.393×10^6	~~−0.06~~ 0.33	~~1.409×10^6~~ 1.393×10^6	~~−0.06~~ 0.33	~~1.407×10^6~~ 1.392×10^6	~~−0.17~~ 0.22
K_{55}	~~7.333×10^7~~ 6.369×10^7	~~7.465×10^7~~ 6.425×10^7	~~1.80~~ 0.88	~~7.465×10^7~~ 6.425×10^7	~~1.80~~ 0.88	~~7.465×10^7~~ 6.425×10^7	~~1.80~~ 0.88
K_{66}	~~8.043×10^5~~ 8.173×10^5	~~8.860×10^5~~ 8.173×10^5	~~10.16~~ 0.01	~~8.950×10^5~~ 8.249×10^5	~~11.29~~ 0.94	~~8.828×10^5~~ 8.145×10^5	~~9.77~~ −0.33
K_{77}	-	~~1.553×10^4~~ 1.534×10^4	-	~~1.553×10^4~~ 1.534×10^4	-	-	-
~~K_{12}~~ ~~-2.308×10^5~~ ~~-2.923×10^5~~ ~~26.68~~ ~~-2.878×10^5~~ ~~24.70~~ ~~- -~~ K_{34}	~~-7.445×10^6~~ -6.675×10^6	~~-7.562×10^6~~ -6.715×10^6	~~1.58~~ 0.60	~~-7.562×10^6~~ -6.715×10^6	~~1.58~~ 0.60	~~-7.562×10^6~~ -6.715×10^6	~~1.58~~ 0.60
K_{35}	~~-9.749×10^7~~ -7.842×10^7	~~-9.807×10^7~~ -7.915×10^7	~~0.59~~ 0.92	~~-9.807×10^7~~ -7.915×10^7	~~0.59~~ 0.92	~~-9.807×10^7~~ -7.915×10^7	~~0.59~~ 0.92
K_{45}	~~1.231×10^6~~	~~1.245×10^6~~	~~1.14~~ 1.86	~~1.245×10^6~~	~~1.14~~ 1.86	~~1.245×10^6~~	~~1.14~~ 1.86

A possible explanation for the slight overestimation of almost all stiffness terms is the different discretization within the tools. The cross-section of PreDoCS is discretized in contour direction only, whereas the BECAScross-section is additionally discretized in thickness direction. The outer contour of both models is the same. BECAS has a more precised discretization of the contour at the corners. In PreDoCS overlapping elements occur at the corners, which are shown as red and yellow elements on the right-hand side of **??**. Due to the overlapping elements the cross-sectional area is overestimated (i. e., excessive material is included in the model) which results in the aforementioned overestimated mass and stiffness terms The shear stiffness terms of Song show high deviations compared to BECAS.

Discretization of the contour for BECAS and PreDoCS

A higher overestimation of about 5 % to 10 % can be observed for the torsional stiffness terms K_{66} for all three calculation approaches which indicates a general difference to BECAS. The analytical approaches take an enclosed area for the determination of the torsional stiffness. In general it is recommended to use the mid-surface line of the enclosed contour, shown as green line in **??**. Due to manufacturing reasons, PreDoCS uses the outer contour as reference line for the layupdefinition as shown in blue in **??**. It can be observed, that the enclosed area is overestimated which leads to an overestimated torsional stiffness. The stiffness terms In all test cases deviations around 20 % for K_{11} and between approximately 100 % and 260 % for K_{22} can be observed, due to the FSDT used by this approach. The Jung approach shows deviations below 5 %, which indicates a significant improvement. The Wiedemann approach does not cover the shear stiffness terms due to its shear-stiff formulation. The deviations of the main stiffness terms for extension (K_{33}) show a deviation to BECAS below 5 %. The bending stiffness terms (), bending (K_{44} and K_{55}) have a deviation up to 14 % but only for the rectangular case . This is caused by the overlapping material in the corners. The part of Steiner of the doubled areas leads to non-proportional deviations caused by the square of the distance. The deviations K_{55}) and torsion (K_{66}) are below 1 % for the Jung approach. The same applies to the Song and Wiedemann approaches except for test case 3 (CUS layup), where deviations up to 10 % occur, which have to be further investigated. The coupling stiffness terms of the Jung and Song approach show a good accordance with the BECAS results. The stiffness term K_{36} for extension-torsion coupling of test case 2 (CUS) is calculated almost exactly. The same applies to the stiffness terms K_{46} and K_{56} for bend-twist coupling of test case 3 (CAS). Similar to the shear stiffness, the coupling terms are not present in the Wiedemann approach.

The deviations for the elastic and shear center given in **??** are table 7 are well below 1 %. .It has to be noticed that the stiffness terms for restrained warping (terms wifth with index 7) are included in the Song and Jung approach but not available in BECAS. Numerical values for warping stiffness terms of closed cross-sections are not provided in literature, neither for beam formulations nor for 2D FE approaches where warping is considered like in VABS (Yu et al., 2005)as described for the VABS code in Yu et al. (2005). Therefore, a study on the effect of warping at the level of a beam structure has needs to be carried out in the future. A comparison of warping displacements and cross-sectional stiffness terms between BECAS and VABS can be found in Blasques (2012).

3.3 Stress distributions

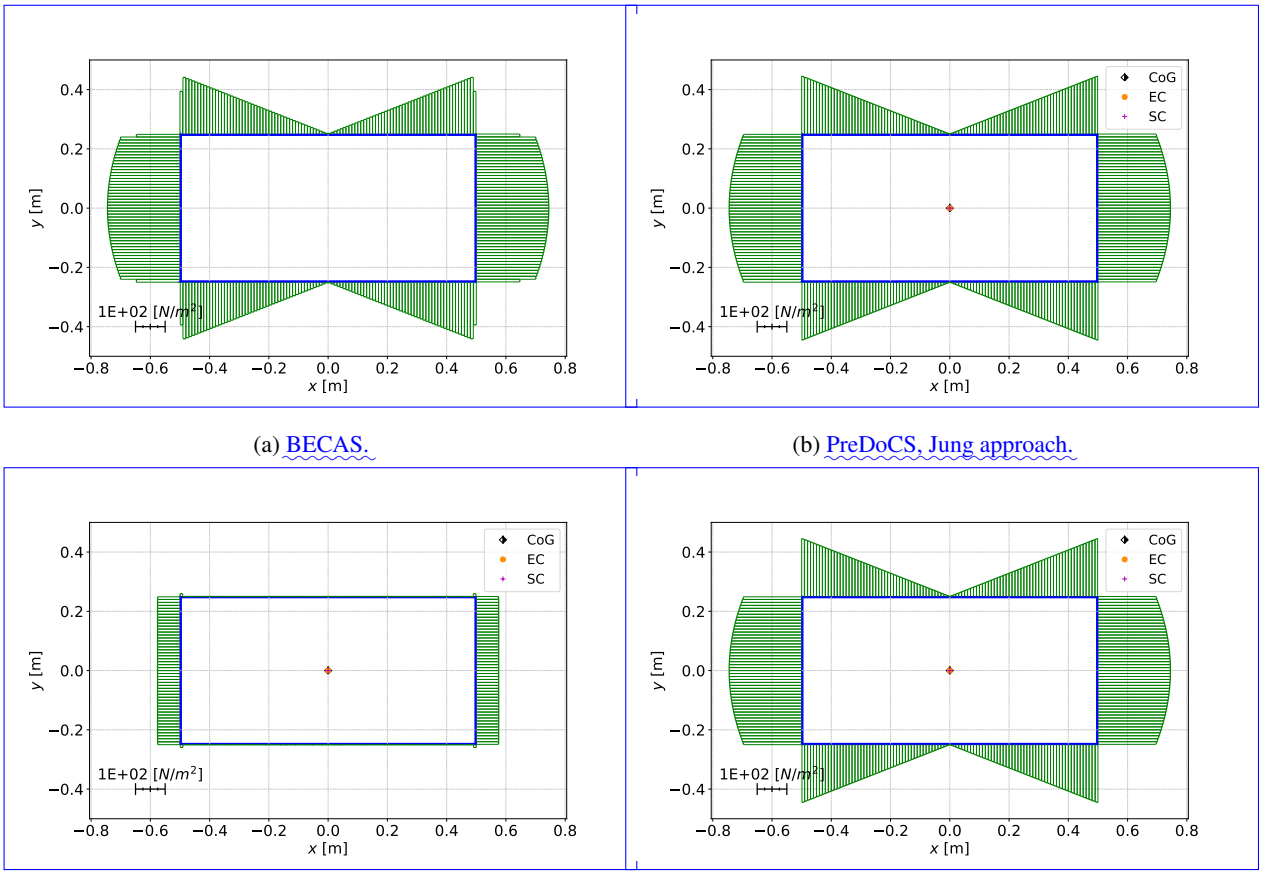

(a) BECAS.

(b) PreDoCS, Jung approach.

(c) PreDoCS, Song approach.

(d) PreDoCS, Wiedemann approach.

Figure 5. Shear stress σ_{zs} distribution for test case 0 under a unit transverse force in y-direction.

~~?? and ??~~ Figures 5 and 6 show a qualitative comparison of the shear stress distributions caused by a transverse force in y-direction.

~~BECAS. PreDoCS, Jung approach. PreDoCS, Song approach. PreDoCS, Wiedemann approach. Shear stress σ_{zs} distribution for test case 900 under a unit transverse force in y-direction.~~

~~BECAS. PreDoCS, Jung approach. PreDoCS, Song approach. PreDoCS, Wiedemann approach. Shear stress σ_{zs} distribution for test case 910 under a unit transverse force in y-direction.~~

A comparison between the three selected approaches for the test cases ~~900~~ 0 (rectangular cross-section) and ~~910~~ 10 (NACA 2412 airfoil) is shown. Furthermore, the Centers of Gravity (CoG), the Elastic Centers (EC) and the Shear Centers (SC) are displayed. ~~The already mentioned differences~~

The differences between the different approaches in the shear stress distributions can be seen very clearly~~between the various approaches. The very~~ . The extraordinarily high deviations of the Song approach result from the ~~usage~~ use of the FSDT, which

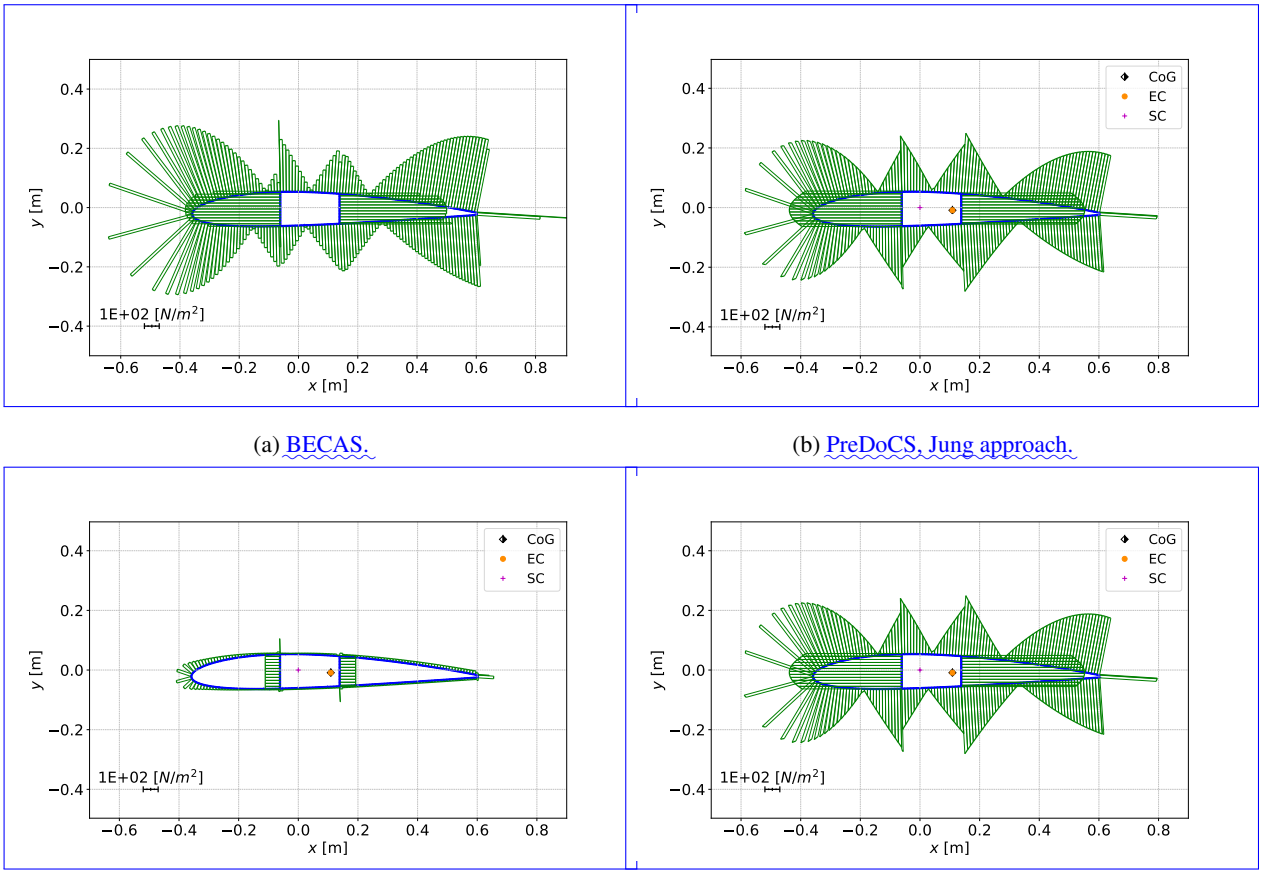

(a) BECAS.

(b) PreDoCS, Jung approach.

(c) PreDoCS, Song approach.

(d) PreDoCS, Wiedemann approach.

Figure 6. Shear stress σ_{zs} distribution for test case 10 under a unit transverse force in y-direction.

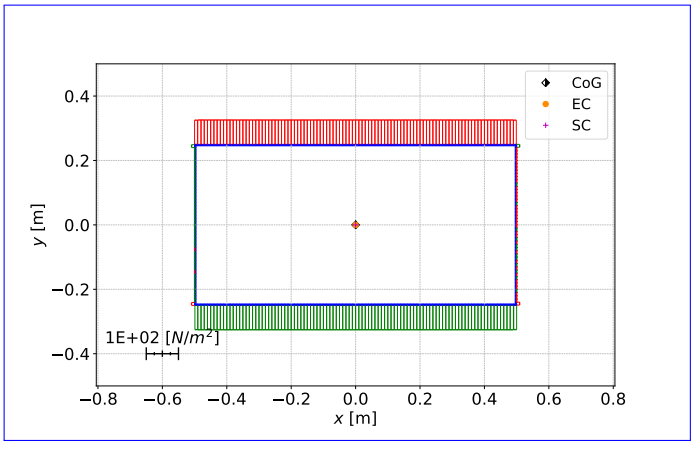

Figure 7. Transverse shear stress σ_{zn} for test case 0 under a unit transverse force in y-direction (Song approach).

assumes a constant shear strain over the entire cross-section. The ~~magnitude of~~ shear stress magnitude using Song's ~~shear stress~~ approach is only a third of ~~the value of the~~ that using the other approaches. This is caused by Song's assumption that the shear stresses occur in the direction of the contour as well as perpendicular to the contour. Combined with the assumption of the FSDT (constant shear strain over the cross-section) and the isotropic material of ~~the test case 900~~test case 0, the horizontal parts of the contour take 2/3 of the ~~transversal~~ transverse force due to ~~the portion of~~ their 2/3 share of the total ~~length of the contour . Therefore~~ contour length. Hence, the vertical parts carry only 1/3, due to the same reason. To illustrate the described effect, the transverse shear stress of the Song approach is shown in ~~??~~fig. 7.

~~Transverse shear stress σ_{zn} distribution for test case 900 under a unit transverse force in y-direction, calculated with the Song approach.~~

~~The~~ The qualitative stress distributions of Jung and Wiedemann show a good ~~accordance~~ agreement with the results from BECAS. ~~A deviation on the webs in test case 910~~ Differences in the absolute values can be observed ~~(see ??). BECAS shows a constant stress distribution due to the discretization of one element along the web whereas the Jung approach shows a quadratic function due to its exact analytical stress function. It has to be noted that for the same discretization,~~ for test case 10 and will be discussed later in the qualitative comparison.

Figure 8 shows the ~~resolution of the stress distribution within the cross-section is significantly higher for the analytical approaches, because the stresses (resp. strains) are returned as function of the circumferential contour coordinate, whereas BECAS provides only one stress value per element due to its 2D FE formulation. To provide an exact stress distribution of a~~ comparison of stress distribution along the contour thickness between BECAS (top) and Jung (bottom) of test case 1 (rectangular cross section with the layup of $(0_2/45/0_2/-45/0_2/45/90/-45/90)_s$). Figure 8a shows the maximum normal stress σ_{zz} under a unit bending around the x-axis, evaluated at the center of the upper edge of the rectangular cross-section~~(as shown in ??), the analytical approaches require only 4 elements (one element per segment line) and can return the stress function or the min. and max. values along one segment. Due to the FE discretization of BECAS more finite elements are needed to get a correct stress distribution (see ??)~~. It can be observed, that the $0°$ plies carry the major portion of the longitudinal load, which is what the $0°$ plies are included for. Figure 8b shows the maximum shear stress σ_{zs} under a unit transverse force in y-direction, evaluated at the center of the left web of the rectangular cross-section. In this case the $\pm 45°$ plies carry the major portion of the shear loads, which is the purpose of the $\pm 45°$ plies. Both figures show very good agreement between the BECAS and Jung solutions.

~~Furthermore a quantitative comparison is~~ A quantitative comparison was carried out and is shown in fig. 9. The ~~distribution~~ distributions of σ_{zz} and σ_{zs} using the analytical approaches are compared with ~~the distribution of these stresses calculated with~~ those using BECAS for all test cases and all load cases (~~transversal~~ transverse force in x ~~-direction~~ direction and y ~~-direction~~direction, extension, bending around the x ~~-axis~~ axis and the y ~~-axis~~axis, torsion). Only the active stresses are considered (σ_{zz} for extension and bending; σ_{zs} for ~~transversal~~ transverse force and torsion), since the reaction stresses become negligibly small and therefore small absolute differences result in very high relative differences. The goal is to represent the deviation of the stress distribution along the complete ~~path~~ contour of the cross-section for one load case and one test case in one single value. ~~Therefore~~ Hence, the absolute value of the relative difference was ~~formed~~ calculated for each element

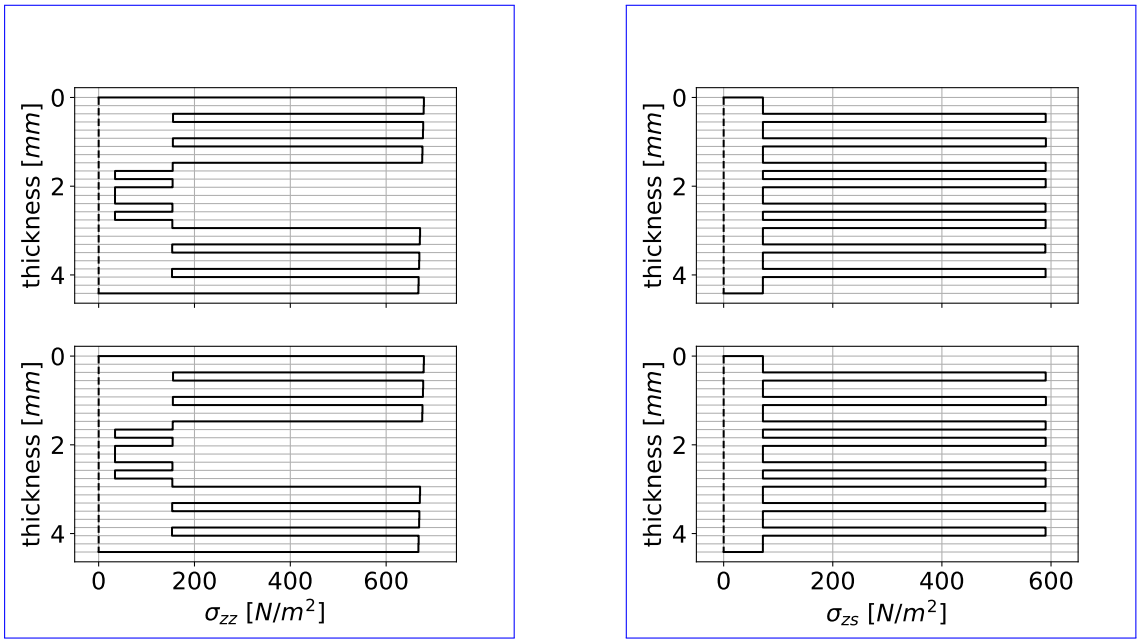

(a) Normal stress σ_{zz} under a unit bending moment around the x-axis, evaluated at the center of the upper edge of test case 1.

(b) Shear stress σ_{zs} under a unit transverse force in y-direction, evaluated at the center of the left web of test case 1.

Figure 8. Comparison of the stress distribution along the contour thickness between BECAS (top) and Jung (bottom).

midpoint of the cross-section, so that negative and positive differences do not cancel out each other. From this "difference distribution", the median is taken as a comparative value, ~~since~~ because it is not strongly influenced by local outliers. ~~Outliers can be caused e.g., by discretization mismatches at the corners of the rectangular cross-section as described in **??**. The medians (orange lines) of relative difference~~ The medians of relative differences for all test case~~- load case -~~/load case combinations are shown in fig. 9 as boxplots[1] grouped by test case, load case and ~~cross-section approach~~calculation method.

Figure 9c shows the already mentioned wrongly calculated shear stress distribution under a transverse force with the Song approach (due to the FSDT used therein). The median of the ~~deviation of the Jung theory is below 7.3 %. Outliers~~ deviations for Jung and Wiedemann are below 1 %. Outliers up to 25 % of the median can be observed for the test cases ~~910 and 911 displayed as small circles~~ 10 and 11 displayed in the upper right corner of fig. 9a. The corresponding load case ~~is a transversal~~ for the Jung approach is transverse load in y ~~-direction~~ direction, shown in fig. 9b~~with the beam at the upper right side. Figure 9c shows that the stress distributions of the Wiedemann theory show a similar deviation for this test cases and load case as those calculated using the Jung approach of about 15 % to 25 % of the median, which needs to be further investigated~~. The shear stress of the analytical approaches are concentrated rather in the webs than in the leading and trailing edge contour compared to BECAS. This effect has to be further investigated.

[1] A boxplot is a graphical representation of data that gives a good overview of the location and scatter of that data. The boxplots used in this paper contain the following statistical data: *Median*: orange line in the box; *Interquartile range*: box; *1.5 times the interquartile range*: "Antennae"; *Outliers*: cricles.

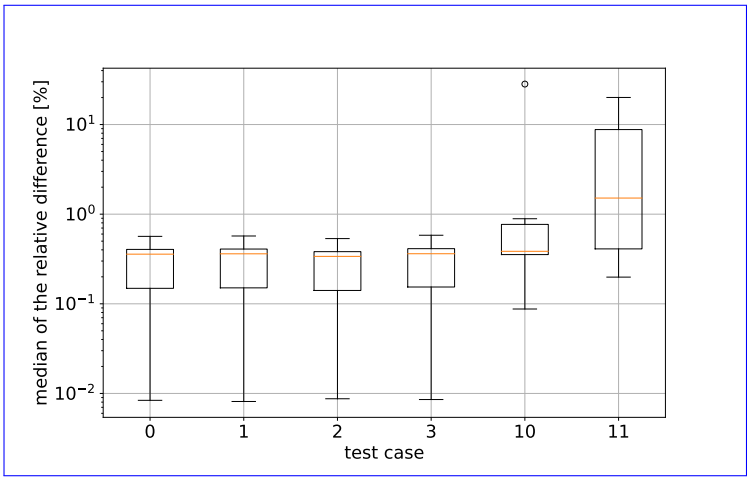

(a) Grouped by test case.

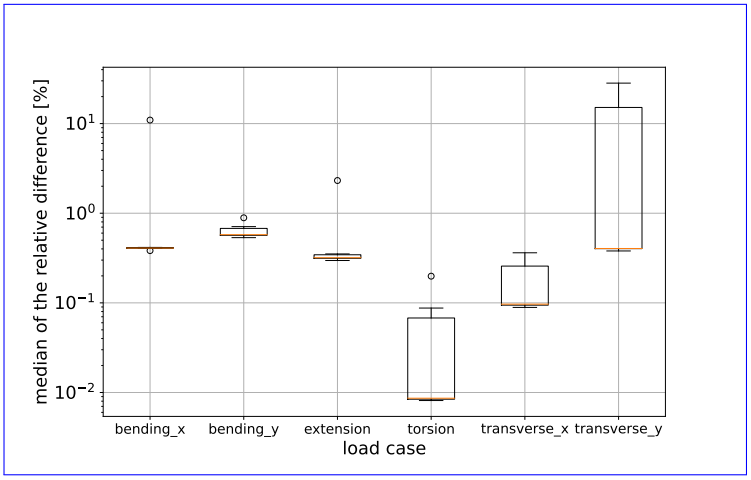

(b) Grouped by load case.

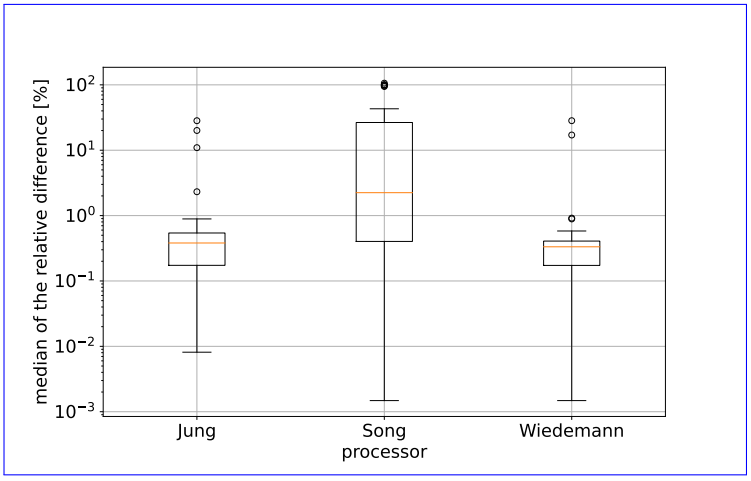

(c) Grouped by cross-section theory.

Figure 9. Boxplots of the median of the relative difference for the active normal and shear stress distributions related to BECAS.

As already mentioned, for an accurate stress distribution of a rectangular cross-section (as shown in fig. 5), the analytical approaches require only 4 elements (one element per edge) and can return the exact stress function along the element or the minimum and maximum values of the element. Due to the FE approach of BECAS, more finite elements are necessary to get a correct stress distribution (see fig. 5). For cross-sections with segments that are not straight, the analytical approaches also need an accurate geometric representation of the cross-section using several elements, but the stress distribution is exact within one element.

3.4 Performance

Table 8 shows the computation time for the calculation of the cross-sectional properties for BECAS and the three implemented cross-section processors in PreDoCS according to the approaches of Jung, Song and Wiedemann. Furthermore the computational time for one load case is displayed. All computations include the time for meshing of the cross-sections. For all approaches the same mesh discretization in contour direction is used (according to table 3) to be able to compare the stress distributions given in fig. 5 and fig. 6. The calculations are executed ~~with~~ on the same PC (Win ~~10~~ 11 64-bit, AMD Ryzen 7 5800H (8 x ~~3.2 - 4.4 GHz), 16 GB~~ 3.2 GHz – 4.4 GHz), 16 GB RAM). The analytical approaches achieve the same accuracy already with 4 elements in contour direction. Further mesh refinement does not affect the stiffness terms and stress distribution. In contrast to that, a fine FE mesh is required in BECAS in order to obtain a converged solution. The resulting benefit by means of computation time savings is shown in the last row of table 8.

It can be observed that for the cross-sectional calculation the ~~analytic~~ analytical approaches are an order of magnitude (partly even more) faster than BECAS. ~~Also the computing time for~~ For a single load case ~~is around an order of magnitudefaster than BECAS~~the difference is around two orders of magnitude. BECAS uses MATLAB which has highly optimized functions for matrix calculations, where a further improvement of the performance is difficult. For ~~the PreDoCScode this optimization of the computation~~ PreDoCS, code optimization has not been done ~~up to now and it is expected to improve the performance further due to usage of packages like Cython ((Behnel et al., 2011))~~yet. Using packages such as Cython (Behnel et al., 2011) will further improve the computation performance. Cython provides the option to compile parts of the Python code as native C-like code which can improve the performance significantly.

~~Furthermore the~~

The time savings need to be ~~analysed~~ further analyzed in the context of a design optimization problem for a complete rotor blade ~~modelled~~ modeled as a beam. Thereby the PreDoCS module has to provide the stiffness and ~~and~~ stress distributions for multiple cross-sections along the span as shown in fig. 10 and multiple load cases. The ~~gained~~ performance improvement per cross-section and load case will therefore add up.

4 Conclusions

The present paper provides an evaluation of different analytical cross-sectional approaches on the basis of requirements derived for the preliminary design of wind turbine blades. The approaches of Wiedemann, Song, and Jung were used to calculate cross-

Table 8. Comparison of the computation time for the calculation of the cross-sectional properties and one load case, compared to BECAS. The last row compares the calculation of the rectangular cross section with a four-element-mesh for PreDoCS.

Approach	Cross-section			Load Case		
	Mean [ms]	Std. dev. [ms]	Diff. [%]	Mean [ms]	Std. dev. [ms]	Diff. [%]
BECAS	~~3628.6~~ 6338.2	~~445.8~~ 847.5		~~71.22~~ 428.4	~~48.47~~ 282.1	
Jung	~~140.0~~ 807.1	~~73.0~~ 30.3	~~−96.1~~ −87.3	~~6.43~~ 5.06	~~9.33~~ 0.95	~~−91.0~~ −98.8
Song	~~96.3~~ 592.4	~~43.0~~ 37.4	~~−97.3~~ −90.7	~~1.46~~ 4.76	~~0.64~~ 0.74	~~−97.9~~ −98.9
Wiedemann	~~37.9~~ 321.2	~~17.3~~ 13.5	~~−99.0~~ −94.9	~~17.96~~ 3.62	~~130.94~~ 0.64	~~−74.8~~ −99.2
Jung (four-element-mesh)	8.48	0.38	−99.87	0.11	0.32	−99.97

sectional stiffness matrices and stress distributions across the cross-section. The results were compared to each other and to the 2D FE-based approach of BECAS, which served as a reference.

Since transverse forces play an important role within the design of rotor blades, the Song approach ~~turns out as not~~ turned out not to be suitable due to the wrongly determined shear stress distribution caused by the ~~usage~~ use of the FSDT. ~~Also the~~ The shear stiffness terms and the related coupling terms ~~are not correctly calculated~~ were also not calculated correctly. The Wiedemann approach ~~does~~ did not cover the coupling and shear stiffness terms at all. It is a simple and fast approach usable only for determining stress distributions, which show ~~a good accordance~~ good agreement with the results from BECAS and Jung.

In terms of accuracy of stiffness terms (also for coupling and shear) and stress distributions, the approach of Jung shows the best results with deviations to BECAS below 5 % (below in most cases), and is therefore taken as cross-section processor in PreDoCS. For ~~test cases 910 and 911 with the transversal load, deviations between 15 % and~~ the stress analyses of test cases 10 and 11, deviations up to 25 % can be observed in ~~this model~~ Jung's model for transversal load in y direction, which have to be further investigated. However, it should be noted that the other analytical models do not predict the transverse shear response better.

The comparison of the approaches on the level of a beam structure w.r.t. overall beam deformations is work in progress~~, especially the evaluation of the influence of~~. The effect of warping also needs to be further investigated. In general, the ~~shear soft formulation (Jung)on the overall beam deformations. The effect of warping also needs to be further investigated.~~ beam

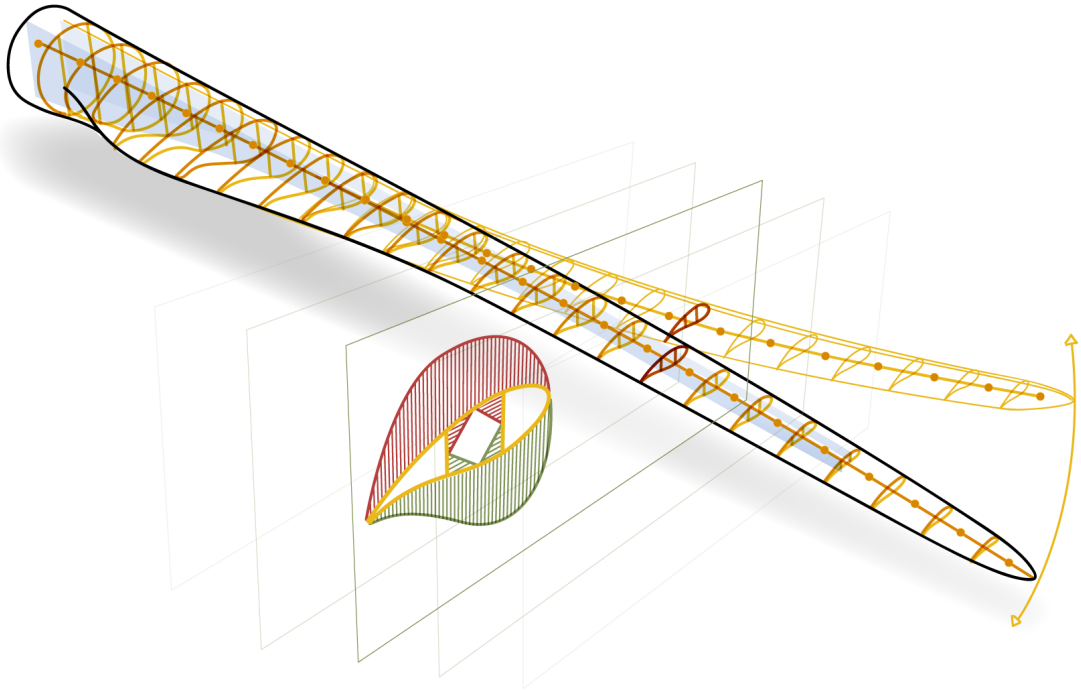

Figure 10. Rotor blade with multiple cross-sections.

model itself must include geometrical non-linearity in the sense of large deflections, as blades undergo very large deflections in operation. Large deflections in turn result in additional coupling effects. For example, when considering equilibrium in the deformed state (which is the definition of geometrical non-linearity), large flap-wise deflections trigger edge-wise bend-twist coupling. If geometric non-linearity would be involved in the beam theory applied for the calculation of the cross-sectional properties, the structural parameters of the cross-sections would need to be updated in each iteration step of the non-linear beam solution, i. e., in each iteration of each time step in the turbine simulation. This could potentially affect the turbine dynamics, which would be interesting to look at. However, this goes far beyond the scope of this paper and may be subject of future work. In any case, such extension would make the turbine simulation very costly, as the number of iterations would increase dramatically.

The presented analytical approaches show a ~~significant~~ significantly better performance with respect to computational time compared to the 2D FE code BECAS. This underlines the usability of analytical cross-section approaches in PreDoCS as solver within a design process where many design candidates need to be evaluated and a high number of design iterations occur. The higher resolution of the stress distribution due to its exact and analytical function of the contour coordinate is easy to differentiate analytically which supports the usage of the approach in gradient-based single- or multi-disciplinary optimization processes with a high number of design variables.

Code availability. The code is open-source available under MIT Licence (Werthen et al., 2023).

Author contributions. EW and DH developed the methodology and software, did the analyses and wrote the manuscript. CB und CH revised the manuscript and provided scientific supervision.

Competing interests. The authors declare that they have no known competing financial interests or personal relationships that could have appeared to influence the work reported in this paper.

Acknowledgements. We would like to acknowledge the funding by the Deutsche Forschungsgemeinschaft (DFG, German Research Foundation) under Germany´s Collaborative Research Center – CRC 1463/1 - Integrated design and operation methodology for offshore megastructures – Project-ID 434502799. Furthermore, we would like to thank the Technical University of Denmark (DTU) for providing BECAS.

References

Behnel, S., Bradshaw, R., Citro, C., Dalcin, L., Seljebotn, D. S., and Smith, K.: Cython: The best of both worlds, Computing in Science & Engineering, 13, 31–39, https://doi.org/10.1109/MCSE.2010.118, 2011.

Bir, G. S.: User's Guide to PreComp (Pre-Processor for Computing Composite Blade Properties), https://doi.org/10.2172/876556, 2006.

Blasques, J.: User's Manual for BECAS: A cross section analysis tool for anisotropic and inhomogeneous beam sections of arbitrary geometry, no. 1785(EN) in Denmark. Forskningscenter Risoe. Risoe-R, Risø DTU – National Laboratory for Sustainable Energy, https://orbit.dtu.dk/en/publications/9a623506-af47-41d6-9d24-5ef0e5b762c1, 2012.

Borri, M., Ghiringhelli, G. L., and Merlini, T.: Composite Beam Analysis Linear Analysis of Naturally Curved and Twisted Anisotropic Beams, http://www.dtic.mil/dtic/tr/fulltext/u2/a252652.pdf, 1992.

Bottasso, C., Campagnolo, F., Croce, A., and Tibaldi, C.: Optimization-based study of bend-twist coupled rotor blades for passive and integrated passive/active load alleviation, Wind Energy, https://doi.org/10.1002/we.1543, 2012.

Carrera, E. and Petrolo, M.: Refined beam elements with only displacement variables and plate/shell capabilities, Meccanica, 47, 537–556, https://doi.org/10.1007/s11012-011-9466-5, 2011.

Chandra, R. and Chopra, I.: Structural behavior of two-cell composite rotor blades with elastic couplings, AIAA Journal, 30, 2914–2921, https://doi.org/10.2514/3.11637, 1992.

Chen, H., Yu, W., and Capellaro, M.: A critical assessment of computer tools for calculating composite wind turbine blade properties, Wind Energy, 13, 497–516, https://doi.org/10.1002/we.372, 2010.

Deo, A. and Yu, W.: Thin-walled composite beam cross-sectional analysis using the mechanics of structure genome, Thin-Walled Structures, 152, 106 663, https://doi.org/10.1016/j.tws.2020.106663, 2020.

Dugas, M.: Ein Beitrag zur Auslegung von Faserverbundtragflügeln im Vorentwurf, https://doi.org/10.18419/opus-3672, 2002.

Gasch, R. and Twele, J.: Wind Power Plants: Fundamentals, Design, Construction and Operation, Springer Berlin Heidelberg, Berlin, Heidelberg, 2nd ed. 2012 edn., 2012.

Giavotto, V., Borri, M., Mantegazza, P., Ghiringhelli, G., Carmaschi, V., Maffioli, G. C., and Mussi, F.: Anisotropic beam theory and applications, Computers & Structures, 16, 403–413, https://doi.org/10.1016/0045-7949(83)90179-7, 1983.

Gjelsvik, A. and Hodges, D. H.: The Theory of Thin-Walled Bars, Journal of Applied Mechanics, 49, 468–468, https://doi.org/10.1115/1.3162198, 1982.

Hodges, D. H.: Nonlinear composite beam theory, American Institute of Aeronautics and Astronautics, https://doi.org/10.2514/4.866821, 2006.

Johnson, E. R., Vasiliev, V. V., and Vasiliev, D. V.: Anisotropic Thin-Walled Beams with Closed Cross-Sectional Contours, AIAA Journal, 39, 2389–2393, https://doi.org/10.2514/2.1247, 2001.

Jung, S. and Nagaraj, V. T.: Structural Behavior of Thin- and Thick-Walled Composite Blades with Multi-Cell Sections, in: 43rd AIAA/ASME/ASCE/AHS/ASC Structures, Structural Dynamics, and Materials Conference, American Institute of Aeronautics and Astronautics, Reston, Virigina, https://doi.org/10.2514/6.2002-1432, 2002.

Jung, S. N. and Park, I. J.: Structural Behavior of Thin- and Thick-Walled Composite Blades with Multicell Sections, 43, 572–581, https://doi.org/10.2514/1.12864, 2005.

Jung, S. N., Nagaraj, V. T., and Chopra, I.: Refined Structural Model for Thin- and Thick-Walled Composite Rotor Blades, AIAA Journal, 40, 105–116, https://doi.org/10.2514/2.1619, 2002.

Kim, C. and White, S. R.: Thick-walled composite beam theory including 3-d elastic effects and torsional warping, International Journal of Solids and Structures, 34, 4237–4259, https://doi.org/10.1016/S0020-7683(96)00072-8, 1997.

Kollár, L. P. and Springer, G. S.: Mechanics of Composite Structures, Cambridge University Press, https://doi.org/10.1017/cbo9780511547140, 2003.

Lee, J.: Flexural analysis of thin-walled composite beams using shear-deformable beam theory, Composite Structures, 70, 212–222, https://doi.org/10.1016/j.compstruct.2004.08.023, 2005.

Lee, S.-L. and Shin, S. J.: Structural design optimization of a wind turbine blade using the genetic algorithm, Engineering Optimization, 54, 2053–2070, https://doi.org/10.1080/0305215X.2021.1973450, 2022.

Libove, C.: Stresses and rate of twist in single-cell thin-walled beams with anisotropic walls, AIAA Journal, 26, 1107–1118, https://doi.org/10.2514/3.10018, 1988.

Librescu, L.: Thin-walled composite beams: Theory and application, vol. 131 of *SpringerLink Bücher*, Springer Netherlands, Dordrecht, https://doi.org/10.1007/1-4020-4203-5, 2006.

Librescu, L. and Song, O.: Behavior of thin-walled beams made of advanced composite materials and incorporating non-classical effects, Applied Mechanics Reviews, 44, S174, https://doi.org/10.1115/1.3121352, 1991.

Maes, V. K., Macquart, T., Weaver, P. M., and Pirrera, A.: Sensitivity of cross-sectional compliance to manufacturing tolerances for wind turbine blades, Wind Energy Science, 9, 165–180, https://doi.org/10.5194/wes-9-165-2024, 2024.

Mansfield, E. H. and Sobey, A. J.: The Fibre Composite Helicopter Blade, Aeronautical Quarterly, 30, 413–449, https://doi.org/10.1017/S0001925900008623, 1979.

Qin, Z. and Librescu, L.: On a shear-deformable theory of anisotropic thin-walled beams: Further contribution and validations, Composite Structures, 56, 345–358, https://doi.org/10.1016/S0263-8223(02)00019-3, 2002.

Rehfield, L. W., Atilgan, A. R., and Hodges, D. H.: Nonclassical Behavior of Thin-Walled Composite Beams with Closed Cross Sections, Journal of the American Helicopter Society, 35, 42–50, https://doi.org/10.4050/JAHS.35.42, 1990.

Rosemeier, M. and Krimmer, A.: Rotorblattstruktur, in: Einführung in die Windenergietechnik, edited by Schaffarczyk, A. P., chap. 5, pp. 169–220, Carl Hanser Verlag GmbH Co. KG, 3 edn., https://doi.org/10.1007/978-3-446-47322-5, 2022.

Saravia, M.: Calculation of the Cross Sectional Properties of Large Wind Turbine Blades, Mecánica Computacional, pp. 3619–3635, http://www.cimec.org.ar/ojs/index.php/mc/issue/view/876, 2016.

Saravia, M. C., Saravia, L. J., and Cortínez, V. H.: A one dimensional discrete approach for the determination of the cross sectional properties of composite rotor blades, Renewable Energy, 80, 713–723, https://doi.org/10.1016/j.renene.2015.02.046, 2015.

Scott, S., Macquart, T., Rodriguez, C., Greaves, P., McKeever, P., Weaver, P., and Pirrera, A.: Preliminary validation of ATOM: an aero-servo-elastic design tool for next generation wind turbines, Journal of Physics: Conference Series, 1222, 012 012, https://doi.org/10.1088/1742-6596/1222/1/012012, 2019.

Scott, S., Greaves, P., Weaver, P. M., Pirrera, A., and Macquart, T.: Efficient structural optimisation of a 20 MW wind turbine blade, Journal of Physics: Conference Series, 1618, 042 025, https://doi.org/10.1088/1742-6596/1618/4/042025, 2020.

Serafeim, G. P., Manolas, D. I., Riziotis, V. A., Chaviaropoulos, P. K., and Saravanos, D. A.: Optimized blade mass reduction of a 10MW-scale wind turbine via combined application of passive control techniques based on flap-edge and bend-twist coupling effects, Journal of Wind Engineering and Industrial Aerodynamics, 225, 105 002, https://doi.org/10.1016/j.jweia.2022.105002, 2022.

Song, O.: Modeling and response analysis of thin-walled beam structures constructed of advanced composite materials, Ph.D. thesis, https://vtechworks.lib.vt.edu/bitstream/10919/38952/1/LD5655.V856_1990.S665.pdf, 1990.

Suresh, J. K. and Nagaraj, V. T.: Higher-order shear deformation theory for thin-walled composite beams, Journal of Aircraft, 33, 978–986, https://doi.org/10.2514/3.47044, 1996.

Vo, T. P. and Lee, J.: Flexural–torsional behavior of thin-walled composite box beams using shear-deformable beam theory, Engineering Structures, 30, 1958–1968, https://doi.org/10.1016/j.engstruct.2007.12.003, 2008.

Wanke, G., Bergami, L., Zahle, F., and Verelst, D. R.: Redesign of an upwind rotor for a downwind configuration: design changes and cost evaluation, Wind Energy Science, 6, 203–220, https://doi.org/10.5194/wes-6-203-2021, 2021.

Weisshaar, T. A.: Aeroelastic Stability and Performance Characteristics of Aircraft with Advanced Composite Sweptforward Wing Structures, http://www.dtic.mil/cgi-bin/GetTRDoc?AD=ADB032318&Location=U2&doc=GetTRDoc.pdf, 1978.

Werthen, E., Hardt, D., and Hühne, C.: PreDoCS: Preliminary Design of Composite Structures, https://doi.org/10.5281/zenodo.10305952, 2023.

Wiedemann, J.: Leichtbau: Elemente und Konstruktion, Klassiker der Technik, Springer-Verlag Berlin Heidelberg, 3. auflage edn., https://doi.org/10.1007/978-3-540-33657-0, 2007.

Yu, W.: Efficient High-Fidelity Simulation of Multibody Systems with Composite Dimensionally Reducible Components, Journal of the American Helicopter Society, 52, 49–57, https://doi.org/10.4050/JAHS.52.49, 2007.

Yu, W., Hodges, D. H., Volovoi, V. V., and Fuchs, E. D.: A generalized Vlasov theory for composite beams, Thin-Walled Structures, 43, 1493–1511, https://doi.org/10.1016/j.tws.2005.02.003, 2005.